To appear as
DESY 06-006
Cockcroft-06-04

Deep Inelastic Electron-Nucleon Scattering at the LHC*

J. B. Dainton[1], M. Klein[2], P. Newman[3], E. Perez[4], F. Willeke[2]

[1] Cockcroft Institute of Accelerator Science and Technology,
Daresbury International Science Park, UK
[2] DESY, Hamburg and Zeuthen, Germany
[3] School of Physics and Astronomy, University of Birmingham, UK
[4] CE Saclay, DSM/DAPNIA/Spp, Gif-sur-Yvette, France

Long version of January 24^{th}, 2006 - for the Orsay Meeting

Abstract

The physics, and a design, of a Large Hadron Electron Collider (LHeC) are sketched. With high luminosity, $10^{33}\mathrm{cm}^{-2}\mathrm{s}^{-1}$, and high energy $\sqrt{s} = 1.4\,\mathrm{TeV}$, such a collider can be built, in which a 70 GeV electron (positron) beam in the LHC tunnel is in collision with one of the LHC hadron beams and which operates simultaneously with the LHC. The LHeC makes possible deep-inelastic lepton-hadron (ep, eD and eA) scattering for momentum transfers Q^2 beyond $10^6\,\mathrm{GeV}^2$ and for Bjorken x down to the 10^{-6}. New sensitivity to the existence of new states of matter, primarily in the lepton-quark sector and in dense Quantum Chromodynamics, is achieved. The precision possible with an electron-hadron experiment brings in addition crucial accuracy in the determination of hadron structure and of parton dynamics at the TeV energy scale. The LHeC thus complements the proton-proton and ion programmes, adds substantial new discovery potential to them and is important for a full understanding of physics in the LHC energy range.

***Contributed to the Open Symposium on European Strategy for Particle Physics Research, LAL Orsay, France, January 30^{th} to February 1^{st}, 2006.**

1 Introduction

Deep-inelastic lepton-hadron scattering (DIS) has long been [1, 2, 3, 4] the most accurate means of exploring the substructure of matter at short distances. Nowadays, such physics is concerned with electron-quark interactions at the highest possible energy and momentum transfer. An ep collider allows new states coupling to leptons and quarks to be produced and their quantum numbers to be determined. It is also concerned with the exploration of new forms of hadronic matter, which may be manifest in very high parton densities at very low Bjorken-x. With an ep collider the parton dynamics and the momentum distributions of quarks and gluons, which are crucial for the discovery and interpretation of new physics, are most accurately determined.

The Large Hadron Collider (LHC) will explore a new range of energy and mass. An ep facility is essential to complete this exploration, both through its unique sensitivity to some possible new states of matter and since it provides complementary information which will be needed to resolve puzzles thrown up by pp and AA data. The most attractive proposition for an ep collider operating in this energy domain is to make use of the 7 TeV LHC p beam by colliding it with an intense electron or positron beam stored in a ring mounted above the LHC, a Large Hadron Electron Collider (LHeC). Compared with linac-ring solutions, such as the ILC with HERA [5] or a CLIC prototype with the LHC [6], this proposition increases the luminosity by two orders of magnitude. An LHeC, in which for example 70 GeV electrons collide with 7 TeV protons, will substantially extend the phase space explored hitherto in deep-inelastic lepton-hadron scattering (Fig. 1).

Deep-inelastic lepton-hadron physics at the TeV scale has been considered previously, at the LEP-LHC workshop in 1990 [7, 8] and as part of the TDR for TESLA in 2001 (THERA) [9]. A ring-ring ep collider using the LHC has been considered based on LEP [10, 11, 12]. This paper is concerned with a new evaluation taking advantage of the experience gained at HERA. A feasibility study for an ep collider at the LHC using an electron ring of energy $E_e = 70\,\mathrm{GeV}$ leads to an estimated luminosity of about $10^{33}\,\mathrm{cm}^{-2}\mathrm{s}^{-1}$, which corresponds to an annual integrated luminosity of about $10\,\mathrm{fb}^{-1}$, at a center of mass (cms) energy of $\sqrt{s} = 2\sqrt{E_e E_p}$ of 1.4 TeV. This places the LHeC very favourably in the luminosity-energy map of DIS physics (Fig. 2).

This paper presents the LHeC for inclusion in the deliberations of the European Strategy Group of the CERN Council [13] during 2006. It highlights LHeC physics with examples and it presents a feasibility study for the machine. The scale of the LHeC is that of an upgrade of the LHC. The next steps are to complete a full evaluation of the feasibility of the LHeC, including injection, and to develop further the optimisation of an experiment and its interface to the machine. The first data at the LHC and the completion of the physics programme at HERA with its final data sample will also have a direct bearing on this optimisation.

The paper is organised as follows: In Section 2 examples are given of new physics at high masses and at very low Bjorken-x. Section 3 is concerned with exploiting the precision of DIS to quantify and test QCD at a new level of accuracy. Section 4

highlights the opportunities at the LHeC to probe QCD in more complex hadronic environments making use of the wide range of ion beams at the LHC. There follows a brief consideration of the kinematic reach and its implications for a detector design in Section 5. Finally, Section 6 is concerned with luminosity prospects based on an initial consideration of the LHeC machine design.

2 New Physics at the LHeC

2.1 Physics Beyond the Standard Model

In the kinematic domain in which the new physics underpinning the Standard Model (SM) is manifest, new electron-quark and positron-quark dynamics could be observable, revealing the relationship between the quark and lepton sectors of the SM. It is this sensitivity to lepton-quark physics at the highest energy and shortest distance, which is a cornerstone of the importance of LHeC.

The high energy of the LHeC extends the kinematic range of DIS physics to much higher values of electron-quark mass $M^2 = sx$ (Fig. 3). An ep collider, providing both baryonic and leptonic quantum numbers in the initial state, is ideally suited to a study of the properties of new bosons possessing couplings to an electron-quark pair in this new mass range. Such particles can be squarks in supersymmetry with R-parity violation ($\not{R}_p$), or first-generation leptoquark (LQ) bosons, which appear naturally in various unifying theories beyond the Standard Model (SM). They are produced as single $s-$channel resonances via the fusion of incoming electrons with quarks in the proton. They are generically referred to as "leptoquarks" in what follows.

Fig. 4 shows the expected sensitivity of the LHC and LHeC colliders for scalar leptoquark production. The single LQ production cross section depends on the unknown coupling λ of the LQ to the electron-quark pair, and means for a coupling λ of $\mathcal{O}(0.1)$, that LQ masses up to 1 TeV could be probed at the LHeC. In pp interactions at the LHC such leptoquarks would be mainly produced via pair production by gluons or singly with a reduced cross section. In ep collisions LQ production can be probed in detail, taking advantage of the formation and decay of systems which can be observed directly as a combination of jet and lepton invariant mass in the final state. It will thereby be possible at the LHeC to probe directly and with high precision the quantum numbers of the perhaps complex structures which will result in the lepton-jet system. Examples follow:

Fermion number (F) : Since the parton densities for u and d at high x are much larger than those for $\bar{u}$ and $\bar{d}$, the production cross section at LHeC of a $F = 0$ ($F = 2$) LQ is much larger in e^+p (e^-p) than in e^-p (e^+p) collisions. A measurement of the asymmetry between the e^+p and e^-p LQ cross sections thus determines the fermion number of the produced leptoquark. Pair production of first generation LQs

at the LHC will not allow this determination. Single LQ production at the LHC [15] , followed by the LQ decay into $e^{\pm}$ and q or $\bar{q}$, could determine F by comparing the signal cross sections with an e^+ and an e^- coming from the resonant state. However, the single LQ production cross section at the LHC is two orders of magnitude lower than at the LHeC (Fig. 5a), so that the asymmetry measured at the LHC will not be statistically significant in a large part of the parameter space. For a coupling $\lambda = 0.1$, no information on F can be extracted from the LHC data for a LQ mass above ~ 700 GeV, while the LHeC can determine F for LQ masses up to 1 TeV (Fig.5b).

Spin: At the LHeC, the angular distribution of the LQ decay products is unambiguously related to its spin. This determination will be much more complicated, even possibly ambiguous, if only the LHC leptoquark pair production data are available. Angular distributions for vector LQs depend strongly on the structure of the $g\,LQ\,\overline{LQ}$ coupling, i.e. on possible anomalous couplings. For a structure similar to that of the γWW vertex, vector LQs produced via $q\bar{q}$ fusion are unpolarised and, because both LQs are produced with the same helicity, the distribution of the LQ production angle will be similar to that of a scalar LQ. The study of LQ spin via single LQ production at the LHC will suffer from the relatively low rates and more complicated backgrounds.

Neutrino decay modes: At the LHeC, there is similar sensitivity for LQ decay into both eq and νq. At the LHC, in pp collisions, LQ decay into neutrino-quark final states is plagued by huge QCD background. At the LHeC, charged current production through eq fusion with subsequent νq decay is thus very important if the complete pattern of LQ decay couplings is to be determined.

Coupling λ: At the LHeC there is large sensitivity down to small values of the coupling λ. With less sensitivity, in pp interactions at the LHC, information can be obtained from single LQ production and also from dilepton production via the t-channel LQ exchange. Since the single LQ production cross sections depend on both λ and the flavour of the quark to which the LQ couples, determining λ and this flavour requires pp and ep data.

Chiral structure of the LQ coupling: Chirality is central to the SM Lagrangian. Polarised electron and positron beams[1] at the LHeC will shed light on the chiral structure of the LQ-e-q couplings. Measurements of a similar nature at LHC are impossible.

Table 1 summarises the observables [16] which could disentangle the various LQ species at an ep machine.

If Supersymmetry is manifest at TeV energy, in ep interactions the associated production of squarks and sleptons ($\tilde{e}$ and $\tilde{\nu_e}$) is via the t-channel exchange of a neutralino or chargino. Fig. 6 shows that the rates can be sizeable at the LHeC when the sum of the squark and slepton masses is below $\sim$ 1 TeV. If squarks are relatively light, ~ 500 GeV, selectron masses up to about 500 GeV could be probed at the LHeC. This may extend somewhat beyond the discovery reach for selectrons in pp scattering at the LHC.

[1] Whether it is possible to achieve longitudinal polarisation in a 70 GeV $e^{\pm}$ beam in the LHC tunnel remains to be clarified.

	$S_{0,L}$	$S_{1,L}$	$\tilde{S}_{0,R}$	$S_{0,R}$	$S_{1/2,L}$	$\tilde{S}_{1/2,L}$	$S_{1/2,R}$
$S_{0,L}$		β_ν	P_e	P_e			
$S_{1,L}$	β_ν		P_e	P_e		e^+/e^-	
$\tilde{S}_{0,R}$	P_e	P_e		$-$			
$S_{0,R}$	P_e	P_e	$-$				
$S_{1/2,L}$						$-$	P_e
$\tilde{S}_{1/2,L}$		e^+/e^-			$-$		P_e
$S_{1/2,R}$					P_e	P_e	

Table 1: Discrimination between LQs with different quantum numbers in $e^{\pm}p$ scattering with an electron beam polarisation P_e. The nomenclature of [17] has been used to label the different scalar LQ species described by the model of Buchmüller, Rückl and Wyler [18], in which the branching ratio β_ν of the LQs to decay into $\nu + q$ is known.

Charge asymmetries and, possibly, polarisation asymmetries could provide additional information on the couplings of the exchanged gauginos and on the mass difference between $\tilde{e}_L$ and $\tilde{e}_R$. Examples of such asymmetries are shown in Fig. 7. Light sfermions are assumed and the framework of the Minimal Supersymmetric Standard Model is used.

2.2 Physics of High Parton Densities (Low x)

The observations at HERA of the rise of the structure function $F_2(x, Q^2)$ and of its derivative $\partial \ln F_2 / \partial \ln Q^2$ as x decreases imply that at low x the sea quark and the gluon distributions, respectively, increase dramatically. At low x proton structure is thus driven by gluons and the formation of quark-antiquark pairs. While the charge of the proton is determined by its valence quarks, the kinetic and potential energy of gluons determines its mass. An understanding of quark-gluon dynamics is thus a key to the mass of the universe [19].

The sharp rise of the density of the gluons in the proton leads to the possibility of non-linear parton interaction effects [20]. A new dense state of parton matter is likely to exist, sometimes referred to as a Colour Glass Condensate [21], which is characterised by a high parton density and small coupling constant.

Much theoretical development in low x physics is concerned with evolution equations which are the most appropriate approximation to a full solution to QCD (such as the BFKL [22], the CCFM [23], and the Balitzky Kovchegov equations [24]), and the incorporation of small x resummation combining the classic DGLAP approach [25] with BFKL evolution [26]. DGLAP theory has been calculated to NNLO [27]. Physics at low x has also been formulated using the colour dipole approach [28]. However, there is still no universally accepted formulation of QCD at low x. This situation can be traced in large part to the fact that the kinematic reach of HERA is insufficient

to establish unambiguously the existence of non-linear parton interaction effects and saturation phenomena [29, 30, 31].

Although the derivative $\partial F_2/\partial \ln x$ shows no evidence for a damping of the growth of the sea quark density with decreasing x, some effects observed at HERA, in forward jet production [32] and in azimuthal (de)correlations [33], seem to indicate departures from the conventional radiation pattern in QCD. Future progress requires the substantial increase of the kinematic reach to low x (Fig. 8) which is made possible by the LHeC.

At the LHC measurements will be performed of the interaction of nuclei, in for example Pb-Pb collisions, with the aim of investigating a high density parton phase (Quark Gluon Plasma). An unambiguous determination of the nuclear parton distributions in the domain accessed with these measurements, which is possible in eA scattering at the LHeC, will be important if the equilibrium of the nucleon (colour singlet) and parton (colour non-singlet, QGP) phases are to be understood. A complete unknown is the gluon distribution in nuclei at low x (Fig. 9) [34].

If, as one expects, the evolution at low x proceeds differently than conventionally assumed, there are important consequences for high energy physics, which reach beyond the intrinsic questions of low x theory. These may include

- the observation of the black disc limit of high energy scattering [35], i.e. of the unitarity limit, which causes the cross sections at high energy to saturate resulting in
- new, possibly radically different, predictions for high energy cosmic ray and neutrino physics, which currently are based on large extrapolations [36], and also
- a different perspective on physics in the forward region of pp, pA and AA interactions at the LHC.

3 Precision Quantum Chromodynamics

QCD is one of the cornerstones of our understanding of the physics of the universe, which is encapsulated in the Standard Model (SM). Like the electroweak sector of the SM, its predictive power depends on the accuracy with which its gauge coupling is known and on our ability to make predictions and compare them with experiment for a variety of hadronic phenomena. Lepton-hadron interactions, in which hadronic matter is probed deeply in a well defined manner, is an extremely powerful means of achieving these aims.

There follow a few examples, in which at the LHeC, because of the precision of an ep experiment and because of kinematic reach, one can foresee a major improvement in the accuracy, with which QCD can be tested, quantified and developed further.

3.1 Structure Functions and Partons for the LHC

Precision measurements at the LHeC of the neutral current (NC) and charged current (CC) deep-inelastic scattering cross sections (Fig. 10) are pivotal in building a successful physics programme at the LHC. Large electroweak effects, which add quark flavour and, through electroweak chirality, matter-antimatter, sensitivity to the well defined deep-inelastic probe, are present (Fig. 11). The primary purpose of these measurements is to extract a number of important structure functions of the proton, and hence to determine a comprehensive set of parton density functions (pdf) for the nucleon. Important examples are the behaviour of the sea and valence quarks at low x, from a measurement of the γZ interference structure function xG_3 (Fig. 12), and the limit of the u/d ratio at large x, from a measurement of charged current $e^{\pm}$ scattering (Fig. 13).

The accuracy with which the parton distributions can be determined contributes directly to the sensitivity to new physics at both the LHC and the LHeC. An example illustrating the accuracy necessary is the measurement to 1% of the luminosity in pp interactions at the LHC using W and Z production [40]. So as to cover the rapidity plateau region at the LHC, it is necessary to know the pdfs of quarks and gluons [41] in the Bjorken-x range 10^{-4} to 0.1 at $Q^2 = M^2_{Z,W} \simeq 10^4$ GeV^2 with adequate precision. This range is covered directly by the LHeC. If HERA data alone are to be used, a large extrapolation is necessary, which requires an accurate understanding of perturbative QCD. The theory underpinning the extrapolation is subtle and far from unambiguous [42]. At large x, resummation effects are important. At low x, the parton dynamics may be non-linear (see section 2.2), and multiple interactions may have to be taken into account when extrapolating to high energy [43].

Furthermore at LHC, heavy quarks play an essential role in QCD dynamics, and thereby their contributions to proton structure must be understood. In particular the bottom quark distribution needs to be known rather accurately because b quarks contribute substantially to the production mechanisms for new physics. With rising Q^2 the fraction of the heavy quark contributions increases (Fig. 14), for b quarks from a few per mil near threshold at HERA [45] to about 5% at the LHeC. Thus with silicon vertex detectors, and taking advantage of the small beam spot size ($15 \cdot 35\,\mu$m^2), very accurate measurements of the beauty and the charm quark densities are possible in a very wide range of Q^2 and x. The greatly enhanced kinematic reach at the LHeC, together with vertex flavour tagging, will make possible measurements of strange and beauty quark densities in the proton using the couplings $sW \to c$ and $bW \to t$ respectively .

Thus, at the LHeC determinations at a new level of precision of all quark distributions in the proton can be anticipated, and, with the combination of the LHeC and HERA structure function measurements, a determination of the gluon distribution in the proton with unprecedented accuracy over an extended range of x will also result.

3.2 Strong Coupling Constant

The strong coupling constant α_s is currently known to 1-2% experimental error. This is much worse than the determination of the fine structure constant and the Fermi

constant, which are known at the level of 10^{-9} and the 10^{-5} respectively. The gravitational constant is known to 0.1%. In unified theories the electromagnetic, weak and strong couplings are expected to approach a common limit. Presently, the accuracy of such extrapolations is limited by the uncertainty with which α_s is known (Fig. 15 [46]). Precision tests of QCD and comparisons with lattice QCD calculations [47] require a significant improvement in the knowledge of α_s.

Deep-inelastic scattering is a well defined process theoretically [1, 48], and has recently been calculated to NNLO [27]. The determination of the strong coupling constant in DIS requires the simultaneous determination of the gluon distribution, xg, and of the quark distributions. At HERA α_s is determined to within an experimental accuracy of about 1% [49]. With the inclusion of the LHeC data, the experimental accuracy is expected to reach a few per mil.

At such a high level accuracy, many theoretical and phenomenological problems also remain to be solved, for example, the treatment of the renormalisation scale uncertainty. By convention[2], one still varies $\mu_r^2 = Q^2$ by factors between 1/4 and 4, which at NLO introduces an uncertainty on α_s of about 5% and at NNLO is estimated to be about 1% [27]. Further examples of theoretical issues which appear at the new level of accuracy with LHeC data are the treatment of heavy flavours in QCD evolution [52] and the limits to the validity of the DGLAP approximation in deep-inelastic scattering [53].

3.3 Hard Diffraction

As discussed in the previous sections, a detailed understanding of physics in the LHC energy range will require substantial developments in the knowledge of Quantum Chromodynamics in the high density, low x, environment. Low x studies at HERA and the Tevatron have shown clearly that diffraction has to be an integral component of any successful low x theory. The contrast between non-diffractive and proton-dissociative DIS, where the proton is rather violently broken up, and diffractive DIS where the proton remains intact, offers a rare experimental window on the mechanism which confines quarks within hadrons.

One of the biggest successes of HERA has been the development of the understanding of diffraction in QCD through the study of the diffractive DIS process (Fig. 16a) $ep \to eXp$ [55]. In this process, the proton remains intact, but loses a fraction $x_{I\!P}$ of its longitudinal momentum in the form of some net colourless partonic system. The virtual photon probes this colourless system, coupling to a quark with a fractional momentum β, in much the same way as the whole proton is probed in inclusive DIS, and producing a diffractive system of mass $M_{\rm X}$. The new kinematic regions and very large luminosities possible at the LHeC make it ideal for further precision study of hard diffraction. Figures 16b and 16c illustrate the dramatic improvements in diffractive kinematic coverage at the LHeC compared with HERA.

[2]Such a large variation of the renormalisation scale is not supported in NLO QCD analyses of the HERA structure function data of H1 [50] and ZEUS [51] and the prescription for estimating the resulting theoretical uncertainty of α_s needs to be reconsidered.

A general framework to describe diffractive DIS is provided by a QCD factorisation theorem [56], which allows "diffractive parton distributions" (dpdfs) to be defined. Such dpdfs have been extracted from the diffractive structure function F_2^D and its scaling violations at HERA [57]. However, unlike the case of inclusive scattering, the dpdfs are only applicable to DIS processes. Large and very poorly constrained "survival" factors are needed before dpdf's can be used to predict pp scattering processes. Testing the factorisation properties and dpdfs extracted at HERA has therefore only been possible thus far by predicting final state DIS observables such as jet or charm cross sections. This approach is heavily limited by the relatively low, accessible, M_X values at HERA (Fig. 16c), which imply that jets can be studied only at uncomfortably low p_t values ($\leq M_X/2$) and that charm cross sections are frustratingly small. The much larger invariant masses accessible at the LHeC would circumvent these problems and would open up new and complementary channels to study, such as diffractive beauty production and diffractive electroweak gauge boson production.

The only way of making significant further constraints and extensions to the dpdfs and studying their QCD evolution is at a higher energy facility such as the LHeC. With the high available luminosities, it will be possible to make measurements in the HERA β range, but at larger Q^2 (Fig. 16b), which would provide a unique opportunity to test the applicability of DGLAP evolution to diffraction.

Fig. 16b also shows a substantial extension towards lower β at the LHeC, similar to that available to lower x in the inclusive case. It is almost certain, that new QCD physics will be observed in this region. The diffractive exchange is often modelled as being derived from a pair of gluons, in which case any novel effects observed in the gluon density should be amplified in the diffraction case.

3.4 Final State Physics

The hadronic final state in deep-inelastic interactions probes details of the **QCD cascade**. While predictions based on the DGLAP evolution equations provide a good description of the current inclusive DIS data, there are indications that this approach might not be sufficient. For example, HERA data on forward jet production at low x show, that non k_t-ordered contributions play an important role. At the LHeC the kinematic domain is extended to much lower x values, providing much greater sensitivity to the topological features of the cascade. With LHeC data various approaches for modeling QCD cascades could thus be distinguished for the first time (Fig. 17) and constraints on the unintegrated parton densities [58] could be obtained. In addition, the increase of the centre of mass energy with respect to HERA will lead to a much larger cross section for heavy flavor production. This would allow the b and c photoproduction cross sections to be measured up to large transverse momentum, providing a much larger level-arm when comparing the measurements to the QCD predictions of the collinear or k_t-factorisation approach [9].

The **hadronic structure of the photon** and its interaction with hadronic matter have long been something of a conundrum. The advent of both e^+e^- and ep colliders in the last two decades, and the huge increases in kinematic reach which have resulted, have meant that it is now possible to see how QCD contributes to the interplay of photon structure and photon interaction dynamics. As a result there is now a phenomenology of hadronic photoproduction (ep) and two-photon production (e^+e^-). A clear distinction between "resolved" and "direct" interactions can be made by means of a Bjorken-x like variable x_γ, which specifies the fraction of the photon momentum participating in the interaction. Resolved photon interactions depend on the structure of the photon, $x_\gamma < 1$, and direct photon interactions correspond to the direct coupling of the photon in a hadronic interaction, $x_\gamma = 1$.

Photoproduction measurements at HERA of hard QCD phenomena (final state transverse momentum squared $p_T^2 > Q^2$) are used to extract structure functions of the photon over a substantial range of Bjorken-x and of photon dimension ($\propto 1/Q$). Features of photon structure, which derive from its underlying $\gamma \to q\overline{q}$ splitting, are now established, and the subtle interplay between the hard scales (Q^2, p_T^2, and when involved a heavy quark mass) are emerging as the photon virtuality, that is its size, changes.

As a result, there now exists a rather comprehensive picture of photon-hadron coupling in terms of QCD for values of x_γ down to about 0.1. Furthermore, the ability to "tune" the nature of the photon interaction between direct and resolved (hadron-like) now begins to throw light on issues in hard hadronic interactions such as multiple parton interactions which would break QCD factorisation. Measurements at LHeC will extend hadronic photoproduction measurements to $x_\gamma \simeq 0.01$ at large momentum transfer, and thus will begin to reveal the properties of the gluon-dominated region of photon structure [9], that is of a flavour singlet object of variable dimension (Q^2).

Prompt photon production, $ep \to \gamma X$, the deep inelastic Compton scattering process, is also sensitive to QCD and photon structure. In the foward region, $\eta_\gamma > 0$, this process is dominated by the reaction $gq \to \gamma q$ with a cross section about an order of magnitude higher at LHeC than at HERA which extends to larger p_t of the photon. Prompt photon production at the LHeC will thus explore the gluon content of the photon [59].

A new way of probing hadronic matter involves the physics of **deeply virtual Compton scattering (DVCS)**, $ep \to ep\gamma$ [60]. Here a parton in the proton absorbs the virtual photon, emits a real photon and the proton ground state is restored. In this process, two gluons at low x (at collider experiments) or two quarks at larger x (as in fixed target experiments), carry different fractions of the initial proton momentum. The DVCS process thus measures generalised parton distributions (GPDs) [**?**] which depend on two momentum fractions x and ξ, as well as on Q^2 and the transfer t at the proton vertex. The DVCS process interferes with Bethe-Heitler scattering, which

allows parton scattering amplitudes to be measured, rather than just cross sections in the form of standard pdfs.

The huge increases in kinematic reach and luminosity with the LHeC will make it possible to build an understanding of proton structure in terms of both transverse (impact parameter or p_T) and longitudinal (rapidity or Bjorken-x) dimensions. Such proton "tomography" [61] will thereby provide a deeper understanding of proton structure. The possibility that DVCS at the LHeC may also be measured in charged current interactions would, like in inclusive scattering, shed light on the variation of flavour structure across the proton dimension.

GPDs can also be accessed in the production of vector mesons [62]. Measurements of the t and W dependence of light (ρ) and heavy ($J/\psi, \Upsilon$) vector meson production will be important means to investigate proton structure and saturation effects at low x at the LHeC.

4 Electron-Nucleus Scattering

4.1 Nuclei

Knowledge of the partonic structure of nuclei is limited to a very small range of x and Q^2 (Fig. 18), and is likely to remain so for the foreseeable future now that there are no plans to develop HERA as an electron-ion collider [63, 64]. The possibilities for eA collisions in the future at lower energy ($\sqrt{s} \leq 100\,\mathrm{GeV}$) at JLab [65] and at BNL [66, 67] will not access the low-x region of nuclear structure, which is crucial to a full understanding of phase equilibria in nuclear matter, that is to the possible existence of a Quark-Gluon Plasma (QGP). Realisation of the LHeC will in contrast put in place a unique tool in the hunt for an understanding of chromodynamic phase equilibria.

The electron-nucleus scattering experiments at the LHeC will have a tremendous impact on the understanding of partonic matter in nuclei and on basic questions of QCD regarding the (de)confinement of quarks [68], the existence of a saturated gluon state, the Colour Glass Condensate [21], and the relationship of nuclear Gribov-Glauber shadowing to hard diffraction [69]. At a certain scale, due to unitarity the rise of the gluon density towards low x has to be tamed, and may not exceed a limit which is estimated to be roughly of the order of Q^2/α_s^2 [9]. Such a limit, illustrated in Fig.19, may have been close to, but not yet reached at, HERA. The limit is likely to be observed in ep scattering at the LHeC and its effects in eA scattering will be large, because the gluon density in nuclei is amplified $\propto A^{1/3}$.

In the regime of very high parton densities, the interaction of small colour singlets with hadronic targets becomes of comparable strength to the geometric cross section πR_A^2 and thus approaches the black disk limit or limit of opacity (absorption). In this limit of large, fixed Q^2 and decreasing x, striking observations are thereby expected in eA DIS [70]:

- a change in the Q^2, x dependence of the structure function, $F_2 \to Q^2/\ln(1/x)$,
- an increased diffractive scattering component approaching to 50% of the inelastic scattering cross section and dominated by dijet production, and
- a much less rapid decrease of the dependence of the cross sections on Q^2 for exclusive vector meson production.

The energy densities achieved in an AA interaction at the LHC are immense, and to fully explore the nature of the interactions will require comparable data in pA, pp, and eA collisions. LHeC and the LHC will thus constitute an experimental tool unparalleled in the history of hadron physics in that nowhere else has there ever been such a range of possible measurements at such an energy scale. Given the importance attached to an understanding of the existence and nature of a QGP, and to the complexities of this understanding, establishing eA physics with the LHeC is of primary value.

4.2 Deuterons

Electron-deuteron scattering complements ep scattering in that it makes possible accurate measurements of neutron structure in the new kinematic range accessed by the LHeC. In a collider configuration, in which the hadron "target" has momentum much larger than the lepton probe, the spectator proton can be tagged and its momentum measured with high resolution [64]. The resulting neutron structure function data are then free of nuclear corrections. For the first time, since diffraction is related to shadowing, one is able to control the shadowing corrections at the per cent level of accuracy [71].

Accurate en cross section measurements will resolve the quark structure of the sea, i.e. the nature of the rise of $F_2^p \propto x(4\bar{u}+\bar{d})$ towards low x, and, from the full set of $e^{\pm}p$ and $e^{\pm}n$ charged current cross section data, unfold the flavour content of the nucleon. For the study of the parton evolution with Q^2, the measurement of $F_2^N = (F_2^p + F_2^n)/2$ is crucial [72] since it disentangles the evolution of the non-singlet and the singlet contributions. This provides additional accuracy in the determination of the strong coupling constant [73].

5 Kinematics and Detector Requirements

The kinematics of inclusive ep scattering is determined from the scattered electron with energy E'_e and polar angle θ_e and from the hadronic final state of energy E_h and a scattering angle θ_h. The negative four-momentum transfer Q^2, the relative energy

transfer y and the Bjorken variable x can be calculated from the scattered electron kinematics as

$$\begin{aligned} Q^2_e &= 4E_e E'_e \cos^2(\frac{\theta_e}{2}) \\ y_e &= 1 - \frac{E'_e}{E_e}\sin^2(\frac{\theta_e}{2}) \end{aligned} \tag{1}$$

and from the hadronic final state kinematics as

$$\begin{aligned} Q^2_h &= \frac{1}{1-y_h}\cdot E^2_h \sin^2(\theta_h) \\ y_h &= \frac{E_h}{E_e}\sin^2(\frac{\theta_h}{2}), \end{aligned} \tag{2}$$

where x is given as Q^2/sy. Note that the angles θ are defined between the directions of the outgoing electron and the proton beam (θ_e) and between the jet and the proton beam (θ_h). The inclusive DIS cross section depends on two variables, besides the cms energy squared $s = 4E_eE_p = Q^2/xy$. The kinematics reconstruction in neutral current scattering is therefore redundant, which is why DIS experiments at ep colliders are precise[3].

Following Eq.2, in charged current scattering the kinematics is reconstructed from the transverse and longitudinal momenta and energy of the final state particles according to [74]

$$\begin{aligned} Q^2_h &= \frac{1}{1-y_h}\sum p^2_t \\ y_h &= \frac{1}{2E_e}\sum (E - p_z). \end{aligned} \tag{3}$$

A feature of this prescription is that losses near the beam pipe in the reconstruction of the kinematics are suppressed because of the factor $\sin^2\theta_h/2$.

The kinematics of ep scattering at the LHeC is illustrated in Fig. 20. Lines of constant energy and angle of the scattered electron and the current jet are located in the (Q^2, x) plane according to the relations:

$$\begin{aligned} Q^2(x, E_e) &= sx(1 - E_e/E_l)/[1 - xE_p/E_l] \\ Q^2(x, E_j) &= sx(1 - E_j/xE_p)/[1 - E_l/(xE_p)] \\ Q^2\ (x, \theta_e) &= sx/[1 + xE_p\cot^2(\theta_e/2)/E_l] \\ Q^2\ (x, \theta_j) &= sx/[1 + E_l\tan^2(\theta_j/2)/xE_p]. \end{aligned} \tag{4}$$

[3]An important example is the calibration of the electromagnetic energy scale from the measurements of the electron and the hadron scattering angles. This leads to energy calibration accuracies for E'_e at the per mil level at HERA, since in a large part of the phase space, around $x = E_e/E_p$, the scattered electron energy is approximately equal to the beam energy, $E'_e \simeq E_e$, which causes a large "kinematic peak" in the scattered electron energy distribution. The hadronic energy scale can be obtained from the transverse momentum balance in NC scattering, $p^e_t \simeq p^h_t$. It is determined to within 1% at HERA.

The accessible kinematic range is limited by the position and dimension of the focussing magnets, see Section 6.7. Limitation of the scattered electron angle to a value $\theta_{e,min}$ defines, for not too small x, a constant minimum Q^2 which is independent of E_p and which is a linear function of E_e^2, $Q^2(x, \theta_{e,min}) \simeq [2E_e \tan^2(\theta_e/2)]^2$. Thus the LHeC, with a rather low electron beam energy of 70 GeV, allows the low Q^2 region to be accessed more easily than THERA [9]. As is illustrated in Fig. 20, roughly a 1° angular cut corresponds to a minimumQ^2 of about 1 GeV^2. To achieve high luminosity, focussing magnets need to be placed close to the interaction region (IR). In the present design an aperture limit of 10° is used. Thus for high luminosity operation, Q^2 reconstructed with electrons is larger than 100 GeV^2.

For THERA a small angle, "backward", electron spectrometer had been sketched [9] using a calorimeter to reconstruct high energies of several hundreds of GeV and a silicon tracker telescope to measure the electron scattering angle down to 179.5° and to identify the electron [9]. The requirements at the LHeC are more modest, because E'_e is lower and the minimum θ_e is larger. At low x the final state and the scattered electron energy add up to approximately the electron beam energy, $E'_e + E_h \simeq E_e$. Final state physics at low x requires access to the region within a few degrees of the beam pipe (Fig. 20). Building a spectrometer for low x physics with a 179(1)° degree acceptance limit for $\theta_e(\theta_h)$ is challenging. The luminosity determination and photoproduction physics require electron and photon tagging detectors to be installed in the electron beam direction.

The increased asymmetry between the electron and proton beam energies at LHeC means that diffractively produced systems are strongly boosted in the outgoing proton direction. The rapidity gap-based diffractive selection, usually employed at HERA, will thus only be effective over a wide $x_{I\!P}$ range if there is substantial instrumentation at large rapidities (up to at least $\eta = 5$). Another intriguing possibility is the use of Roman pots, which are planned for the LHC at the TOTEM experiment [75] and which are proposed in connection with ATLAS and CMS in the FP420 project [76].

At larger Q^2 the electron is scattered to angles between 170° and 10° with energies between about 10 GeV and a few TeV. A minimum angle cut $\theta_{h,min}$ in the forward region, the direction of the proton beam, excludes the large x region from the hadronic final state acceptance (Fig. 20), along a line $Q^2\ (x, \theta_{h,min}) \simeq [2E_p x \tan^2(\theta_{h,min}/2)]^2$, which is linear in the $\log Q^2$, $\log x$ plot and depends on E_p only. Thus at $E_p = 7$ TeV the minimum Q^2 is roughly $(1000[500]x)^2$ at a minimum angle of 10[5]°. Since this dependence is quadratic with E_p, lowering the proton beam energy may be of interest for reaching the highest possible x. As is seen in Fig. 20, the high luminosity IR will have full coverage of the final state up to largest y. The final state energies vary between about 20 GeV at $Q^2 \simeq 100$ GeV^2 and reach a few TeV at large x. The central detector thus needs a strong solenoidal field, silicon and gaseous tracking detectors and a calorimeter capable of reconstructing electromagnetic and hadronic energy from a few tens of GeV up to a few TeV energies. Accurate muon identification and momentum measurement is crucial for new physics at the LHeC to be explored.

Issues on the interaction region (IR) and detector requirements were discussed previously at the LEP-LHC workshop [11, 7], which was held prior to the startup of

HERA. Certainly the interface of the interaction region described below with an *ep* detector and its design will require much more detailed investigations then were aimed at and possible at this stage.

6 Luminosity Prospects for the LHeC

6.1 Introduction

In the following the possibilities are explored for achieving a high luminosity of lepton-proton collisions using the existing LHC proton beam together with a new lepton storage ring in the LHC tunnel while maintaining the existing facility for proton-proton collisions. Earlier studies [77, 9] of possible lepton-proton colliders, which considered a configuration of a proton storage ring and a lepton linac, yielded a relatively small luminosity. Using the expressions derived in references [77, 9] for the case of collisions between the LHC proton beam and a high energy lepton beam produced by a linear accelerator, the luminosity is given by

$$L = 4.8 \times 10^{30} \cdot cm^{-2}s^{-1} \frac{N_p}{10^{11}} \cdot \frac{10^{-6}m}{\varepsilon_p} \cdot \frac{\gamma_p}{1066} \cdot \frac{10cm}{\beta_p^*} \cdot \frac{P_e}{22.6MW} \cdot \frac{250GeV}{E_e} \qquad (5)$$

Assuming the so-called "ultimate" LHC parameters [78] with the number of protons per bunch $N_p = 1.67 \cdot 10^{11}$, the normalized proton transverse emittances of $\varepsilon_{pN} = 3.75 \cdot 10^{-6}$m, a proton beta function β_p^* of 0.5 m at the interaction point, a proton beam energy of 7 TeV, (corresponding to a Lorentz-factor of $\gamma_p = 7460$) and assuming a lepton energy of E_e =70 GeV and an available electron beam power of $P_e = 50$ MW one expects peak luminosities of $L = 2.4 \cdot 10^{31}\mathrm{cm}^{-2}\mathrm{s}^{-1}$ for a ring-linac solution. The luminosity could be increased somewhat by reducing the proton emittance by using transverse cooling. The cooling of the bright and very high energy proton beams of the LHC is considered to be very challenging as experimental verification of proton beam cooling at these high energies has yet to be demonstrated. It thus seems worthwhile to reconsider the luminosity which could be achieved in a ring-ring configuration, using the LHC to accommodate an additional lepton storage ring, which would be installed above the existing superconducting magnets of the LHC and which would be brought into collisions with the LHC proton beam in one interaction point.

Similar estimates have been performed previously [10, 12]. The present estimate makes explicit use of the available experience of high luminosity operation at the circular lepton-proton collider HERA to derive a realistic scaling of the achievable luminosity of a ring-ring-based lepton proton collider in the LHC tunnel.

The aim of the present study is to investigate the parameters required for a realistic LHeC with a peak luminosity of $L = 10^{33}\mathrm{cm}^{-2}\mathrm{s}^{-1}$ while maintaining the option for continued operations with proton-proton collisions.

The present study does not purport to be exhaustive in that detailed designs of the lattice, investigations of beam stability, and conceptual designs of accelerator components have not been performed. However, no limitations associated with these issues are foreseen as similar systems have been demonstrated in existing accelerators or will be demonstrated soon. In particular there is no detailed design of the magnets in the lepton-proton interaction region (IR) or the layout of and other accelerator hardware systems. The injector system is assumed to be identical to the LEP injector system.

6.2 General Requirements

The present study of the LHeC is based on the following general requirements and assumptions:

- A high luminosity in the order of $L = 10^{33}\mathrm{cm}^{-2}\mathrm{s}^{-1}$ is assumed necessary to perform the physics program in a reasonable amount of time.
- The electron beam energy should be as high as possible to obtain a large centre of mass energy which exceeds the HERA centre of mass energy of 318 GeV by a significant factor. The choice of the centre of mass energy is motivated by the physics and is a sensitive parameter for the achievable luminosity. For this study values of around $E_{cm} = 1.4$ TeV were explored corresponding to an electron beam energy of 70 GeV given a proton beam energy of 7 TeV.
- It appears to be highly desirable to find a solution which allows for proton-proton collisions in the interactions regions (IR) of the LHC denoted by IR 1 and IR 5 during lepton proton collision operation. This implies that the parameters of the proton beam should correspond as much as possible to the LHC beam parameters.
- This implies also that the proton beam parameters for LHeC are already predetermined by the design for the LHC. The parameters used in this study are listed in Tab. 2 from [78].
- In order to provide sufficient space and acceptance for the experimental detector, a magnet-free space of at least 2.4 m is required in the interaction region. The aperture of the first accelerator lattice elements should allow for a detector acceptance angle of 10 degrees.
- The electric power consumption of the LHeC should be in a reasonable range compared to the CERN overall power consumption.

Table 2: LHC proton beam parameters used in this study

Proton Beam Energy	TeV	7
Circumference	m	26658.883
Number of Protons per bunch	10^{11}	1.67
Normalized transverse emittance	μm	3.75
Bunch length	cm	7.55
Bunch spacing	ns	25

6.3 Overall Parameters of the LHeC

The luminosity of a high energy proton-lepton circular collider, expressed in terms of the limiting parameters is given by

$$L = \frac{I_e \cdot N_p \cdot \gamma_p}{4 \cdot \pi \cdot e \cdot \varepsilon_{Np} \sqrt{\beta_{xp} \beta_{yp}}}. \tag{6}$$

In this equation, I_e is the total lepton beam current, N_p is the number of protons per bunch, γ_p is the Lorentz factor of the protons and represents the proton beam energy, ε_{Np} is the normalized proton transverse beam emittance (which is assumed to be equal in both planes) and β_{xp} and β_{yp} are the values of the proton beam amplitude function (β-function) at the interaction point (IP). Implicit in this formula are the requirements that the beam cross sections σ of the proton and lepton beams at the IP be equal, $\sigma_{xp} = \sigma_{xe}$, $\sigma_{ye} = \sigma_{ye}$, which is concluded from experience at the SPS and HERA [79], and that the beam-beam tune shift parameters are in a tolerable range, which is particularly relevant for the lepton beam.

The proton beam parameters are assumed to be identical to the so-called "ultimate" LHC proton beam parameters with the beam energy of 7 TeV, the number of protons per bunch N_p= $1.67 \cdot 10^{11}$, and the normalized emittances of $\varepsilon_{Np} = 3.75 \cdot 10^{-6}$m. Given the aforementioned constraints, to achieve a luminosity of $L = 1 \cdot 10^{33}\text{cm}^{-2}\text{s}^{-1}$, only the total lepton beam current I_e and the beta-functions at the IP remain as free parameters.

The maximum lepton beam current in a high energy lepton storage ring is limited by the available RF power. Other potential limitations, such as the dissipation of this power around the accelerator or localized heating due to higher-order modes, can be avoided by an appropriate design of accelerator components. The total output RF power is typically limited by cost: an RF output power of P_{rf}= 50 MW (which is approximately 86% of the LEP power consumption or 28% of the 1999 CERN site power consumption of 910 GWh [80] assuming a yearly operating time of 5000 h) is considered here (somewhat arbitrarily) to be an upper limit. Since the basic ring parameters can only be varied slightly, the maximum lepton beam current is then determined by the lepton beam energy. A lepton which travels with an energy of E_e around the ring with a bend radius of ρ =3133 m incurs an energy loss per turn of $e\Delta U = C_g E_e^4 / (e\rho)$

(C_g =4/3 $\pi r_0 E_0^{-3}$ =8.821 $\cdot 10^{-5}$ GeV^{-3}m) [81]. For a given available power, the total beam current is

$$I_e = 0.351mA \cdot (P_{rf}/MW) \cdot (100GeV/E_e)^4, \tag{7}$$

with $E_e = 70\,\mathrm{GeV}$, $P_{rf} = 50\,\mathrm{MeV}$ and assuming quasi loss-free superconducting RF resonators, the total beam current is $I_e = 74\,\mathrm{mA}$.

With the proton beam parameters, the RF power and the lepton beam energy fixed, it remains to design the interaction region and a lepton accelerator lattice, which provides proton beta functions at the IP of at most $\beta_{xp}\beta_{yp} = 1m^2$, and which allows to match the cross section of the lepton beam while providing sufficient dynamic aperture.

The lepton emittance determines the lepton beta functions at the IP since the beam cross sections need to be matched $\beta_e = \beta_p \epsilon_p/\epsilon_e$. The choice of the lepton beam emittance is constrained to a window limited by dynamic and geometric aperture considerations and beam-beam tune shift limitations.

The lepton emittance should be sufficiently small to avoid a too large maximum beta function in the low beta quadrupoles. The beta function at the IP, β^*, also determines the natural chromaticity contributions from the interaction region

$$\xi_{IP} \simeq 2/\pi \cdot D_{eff}/\beta^*, \tag{8}$$

where D_{eff} is the effective distance of the low beta quadrupoles from the IP. If the chromaticity contributions from the IR exceed a certain fraction of the contributions from the arc

$$\xi_{arc} = N_{cell}/\tan(\Phi_{cell}/2)/\pi \tag{9}$$

[82], the dynamic aperture becomes a critical issue [83] according to experience at HERA where the critical fraction is about $f = \xi_{IP}/\xi_{arc} = 0.4$ [84] (LEP: 0.5 [85]). Here N_{cell} is the number of FODO cells, Φ_{cell} is the betatron phase advance per FODO cell. With these considerations the limiting value of the horizontal lepton emittance for matched beam cross sections is given by

$$\xi_r < f\xi_{arc} \rightarrow \epsilon^e_{x,y} < \frac{f N_{cell} \tan(\Phi_{cell}/2) \cdot \beta^p_{x,y}\epsilon_p}{2D_{eff}} \tag{10}$$

With a LEP-like lattice and $N_{cell} = 290$, assuming an effective $D_{eff} = 3\,\mathrm{m}$, and assuming the horizontal beta functions of the protons to be approximately four times larger than the vertical, i.e. $\beta_{xp} = 1.8\,\mathrm{m}$, one obtains for the emittances limiting values of $\epsilon^e_x = 18\,\mathrm{nm}$, $\epsilon^e_y = 5\,\mathrm{n}$. Since this small ϵ^e_x value cannot be achieved, even with the strongest focusing in a LEP-like structure [86], the number of FODO cells N_{cell} should be increased. In this way the limiting value increases and the achievable minimum emittance reduces because of the shorter FODO cell length. A more acceptable choice for the number of cells is $N_{cell} = 480$. The limiting value of the emittance for good dynamic aperture is then $\epsilon^e_x < 29\,\mathrm{nm}$ which is expected to be easily achievable with an appropriate lattice design.

The other limitation on the emittance of the lepton beam is due to the beam-beam effect suffered by the lepton beam and which is parameterized by the linear tune shift parameter

$$\Delta\nu^e_{x,y} = \frac{\gamma_p r_0 N_p \beta^e_{x,y}}{2\pi\gamma_e \cdot \varepsilon^p_N \cdot \sqrt{\beta^p_{x,y}}(\sqrt{\beta^p_x} + \sqrt{\beta^p_y})} = \frac{r_0 N_p \sqrt{\beta^p_{x,y}}}{2\pi\gamma_e \cdot \varepsilon^e_{x,y}(\sqrt{\beta^p_x} + \sqrt{\beta^p_y})} \tag{11}$$

(r_0 classical electron radius). Tune shift parameters, which have been achieved in HERA, are $\Delta\nu^{He}_y = 0.05$ and $\Delta\nu^{He}_x = 0.03$ [87, 88]. The corresponding limit on the lepton beam emittances depends on the ratio of the proton beta functions at the IP, $r_\beta = \sqrt{\beta_{xp}/\beta_{yp}}$, the only free parameter left:

$$\varepsilon^e_x = \frac{r_0 N_p \cdot r_\beta}{2\pi\gamma_e \Delta\nu^{He}_x (1 + r_\beta)} \tag{12}$$

$$\varepsilon^e_y = \frac{r_0 N_p}{2\pi\gamma_e \Delta\nu^{He}_y (1 + r_\beta)} \tag{13}$$

For $r_\beta = 2$ one obtains emittance limits of $\epsilon^e_x = 12\,\text{nm}$ and $\epsilon^e_y = 4\,\text{nm}$, respectively. Based on these considerations, the horizontal emittance for the lepton accelerator in LHeC is chosen to be $\epsilon^e_x = 26\,\text{nm}$ while the vertical emittance value is 5 nm, assuming a coupling of 20%. Assuming a ratio $r_\beta = 2$ implies lepton β-functions at the IP of $\beta_{xe} = 3.8\,\text{cm}$ and $\beta_{ye} = 5\,\text{cm}$.

The main parameters which are implied by the above considerations are listed in Tab. 3.

Table 3: Main Parameters of the Lepton-Proton Collider

Property	Unit	Leptons	Protons
Beam Energies	GeV	70	7000
Center of Mass Energy	GeV	1400	
Total Beam Current	mA	66.6	544
Number of Particles / bunch	10^{10}	1.04	17.0
Bunch frequency / bunch spacing	MHz / ns	40 / 25	
Horizontal Beam Emittance	nm	25.9	0.501
Vertical Beam Emittance	nm	5	0.501
Horizontal β-functions at IP	cm	3.77	180
Vertical β-function at the IP	cm	4.44	50
Energy loss per turn	GeV	0.676	$6 \cdot 10^{-6}$
Radiated Energy	MW	50	0.003
Luminosity	$10^{33}\text{cm}^{-2}\text{s}^{-1}$	1.04	

6.4 Lepton Ring

A detailed design of an electron ring has not been carried out. The parameters of the lepton storage ring of the lepton proton collider are chosen to be as close as possible to those of LEP [86], which was housed in the LHC tunnel.

The accelerator lattice consists of a FODO structure in the eight arcs with a betatron phase advance per cell of $\phi_{cell} = 108^\circ$ in the horizontal plane and 90 degrees in the vertical plane. The cell length is $L_{cell} = 47.214$m and the bending radius is $\rho = 3133.252$ m. The ring has a circumference of C =26658.876 m. To further reduce the horizontal emittance, the damping distribution will be changed in addition to the strong focusing. The ring will be operated with a relative shift of the RF frequency of $\Delta f/f_{RF} = 4.11{\cdot}10^{-7}$ which corresponds to an energy shift of $\Delta E/E = -1.99 \cdot 10^{-3}$. This changes the damping partition numbers in favour of horizontal damping to a value of J_x= 2.49 and yields a beam emittance ε_{ex} of 25.89 nm at 70 GeV. The corresponding lepton beam energy spread is $(\delta E/E)_{RMS} = 2.06{\cdot}10^{-3}$.

The beam current of 74 mA is composed of 3555 bunches (not counting for an appropriate abort gap) spaced by 25 ns with $1.38 \cdot 10^{10}$ particles in each bunch.

With the bend radius of 3133 m, a 70 GeV electron (positron) will suffer an energy loss of 676 MeV per turn by the emission of synchrotron radiation with a critical energy of 254 keV. The power loss of a beam of 74 mA amounts to 50 MW. The linear power load to the vacuum system is 26 W/cm. This is a large but feasible value. It exceeds the values of HERA (5.2 MW dissipated over 3818 m yielding 13.5 W/cm) by about a factor of two. The cooling system used at HERA is both conservative and conventional. The values for LEP were 9 Wcm^{-1} with a critical energy of 522 keV for beam energy of 100 GeV and a beam current of 12 mA [89].

The RF system is assumed to consist of superconducting 1GHz RF resonators with an accelerating gradient of 12 MV/m. An active RF structure length of 100m or 670 resonator cells is required to produce a total voltage of 1327 MV. This voltage allows a synchronous phase of 31 degrees and provides an RF bucket which accommodates ten times the RMS beam energy spread. This is expected to provide sufficient margin for a good beam lifetime. The parameters of the lepton ring are summarized in Tab 4.

Proven superconducting RF technology for lepton storage rings exists for only half the envisioned RF gradient [90]. However, design efforts for superconducting RF for continuous operation (CW), for large beam currents and high bunch intensities are underway for ERL and CW-LINAC applications (see for example [91]). The corresponding designs could serve as a starting point for an appropriate layout of a LHeC RF system. More development is required in the design of input couplers and higher order mode couplers.

Geometrical considerations need to be taken into account in accommodating an additional lepton ring in the existing LHC tunnel. In the arc sections there appears to be sufficient space to place the lepton beam line above the LHC magnets. In the

straight section, it may be cumbersome to accommodate the large RF systems of the lepton ring.

Since the ATLAS and CMS detectors are assumed to remain active at their locations when the lepton-proton collider is operated, a bypass must be provided around the CMS and ATLAS detectors. There exist survey tunnels which are in parallel with the LHC straight sections 1 and 5 which could be used to bypass the caverns which house the experimental detectors. They have a distance of about 10 m from the LHC beam axis and a length of about 100 m. Two ≈ 250 m long, up to 2 m diameter connection tunnels would have to be drilled from the end of the arcs to connect to these tunnels (see sketch in Fig. 21).

Lepton beam instabilities are not expected to become an important performance limitation given that the design single bunch currents are relatively modest. The expected total impedance, roughly estimated, is less than the impedance of LEP. The bunch population is much lower than the one in LEP. For this reason, there should be no single bunch beam current limitations. A conventional active damper system could be used to damp coupled bunch oscillations if needed.

An open issue concerns the dynamic aperture of the lepton ring taking into account the contributions of the chromaticity in the interaction region. In this design study the beam emittance has been derived using scaling laws. Dynamic aperture studies will be necessary to assure sufficient stability.

6.5 Interaction Region

The electron-proton interaction region is taken to be installed in one of the existing LHC straight sections. The main detectors CMS and ATLAS are assumed to remain active during the operation of the lepton proton collider thus excluding the possibility of lepton-proton collisions in the straight sections around IP5 and IP1. The straight sections around IP7 and IP3 are needed for beam cleaning, which cannot be compromised for LHC proton operation. IP4 and IP6 are occupied by the proton RF and beam dump systems. This leaves only IP2 which is occupied by the ALICE detector and IP8 which is occupied by LHCb. Likely, a lepton-proton physics programme at the LHC would be performed after the B-physics programme is completed. In this case one may envisage an interaction region for the LHeC around IP 8 (Fig. 22).

In order to provide small beta, the low beta quadrupole magnets have to be reasonably close to the IP. This requires a quick separation of the two beams outside the collision region. Separation by strong magnetic fields produces high power synchrotron radiation which is a large problem because of experimental backgrounds and heating of the vacuum system. The alternative, a large crossing angle reduces the luminosity. The IR design has to compromise between these difficulties.

In order to allow for simultaneous lepton-proton and proton-proton operation, the following collision scheme is proposed: The lepton bunch spacing is 25 nm, which is

Table 4: Parameters of the electron ring accelerator

Electron Ring Parameters		
Parameter	Unit	Value
Circumference C	m	26658.86
Beam Energy E_e	GeV	70
Arc Focusing		FODO
Cell length L_c	m	55.87
Bending radius $g\rho$	m	3133.252
Horizontal betatron Phase Adv./cell $\Delta\phi_x$	degree	108
Vertical betatron Phase Adv./cell $\Delta\phi_y$	2π	90
Number of FODO cells in the Arcs N_{cell}		480
Arc Chromaticity (hor/vert.) $\xi_{x,y}$		165/153
Beam Current I_e	mA	74
Bunch distance τ_b	ns	25
Number of bunches n_b		3555
Number of particles per bunch N_e	10^{10}	1.04
Momentum compaction factor α	10^{-4}	0.739
Horizontal beam emittance ε_{xe}	nm	25.9
Vertical beam emittance ε_{ye}	nm	5
RMS energy spread σ_e	10^{-3}	2.06
RMS bunch length	mm	4.5
Particle Radiation energy loss per turn eU_{loss}	MeV/turn	684
Beam Power loss P_{loss}	MW	50
Circumferencial Voltage U	MV	1327
Synchronous Phase ϕ_{synch}	degree	34.6
RF frequency f_{rf}	MHz	1000
Bucket height h_b	σ_e	10.2
RF frequency shift	Hz	300
Synchrotron frequency f_s	f_{rev}	0.13

the nominal LHC proton bunch spacing. The two proton beams would traverse the low beta quadrupoles of the lepton beam and would traverse the IP with a relative angle of 3.5 mrad in the horizontal plane. The non-colliding proton bunch is vertically displaced thus providing a vertical separation to the lepton and colliding proton beam. The lepton beam would traverse the IP with an angle of θ_c= 0.5 mrad in the horizontal plane relative to the colliding and non-colliding proton beam.

The interaction region design is thus based on a small horizontal crossing angle of 0.5 mrad. This implies that the interaction geometry is anti-symmetric around the interaction point which leads to a narrower synchrotron radiation fan. This helps with the collimation scheme. The crossing angle avoids large synchrotron radiation power to be dissipated in the cold beam pipes of the proton low-beta quadrupoles. To regain the associated luminosity reduction by a factor of 1.66 caused by the crossing angle, so-called crab-crossing is assumed which requires a tilt of the proton bunches around a vertical axis. This is discussed further below.

At the first parasitic *ep* collision point at 11.25 m from the IP, the lepton and the proton beam are separated by about 12 mm or 8.2 σ of the horizontal lepton beam size. This separation is considered sufficient to avoid potentially harmful interactions due to so-called parasitic crossings.

The length of the magnet-free space for the detector beam-pipe is assumed to be 1.2 m. The space requirement for the first low beta quadrupole of the lepton beam is 400 mm in diameter. This provides a detector acceptance angle of 9.4° around the longitudinal axis.

The low beta quadrupole magnets for both protons and leptons are assumed to be superconducting. The focusing of the electron beam could be accomplished using a low-beta quadrupole triplet located at a distance of 1.2 m from the IP followed by an 50 m long drift without focusing elements. The superconducting low beta quadrupole magnets have a gradient of 93 T/m, lengths of 96 cm, 204 cm and 114 cm respectively and they provide half apertures of 30 mm, 40 mm and 55 mm.

The beam separation is accomplished as follows: The low beta quadruples are displaced by 0.35 mm from the beam axis which constitutes a 4.15 m long soft separating magnetic field which provides a deflection of 0.5 mrad. The low beta triplet is followed by a long soft separator dipole magnet with a field of only 0.033 T and a length of 15 m. The separation provided by this magnet is 2.1 mrad. This arrangement, together with the crossing angle of 0.5 mrad provides a beam separation of 40 mm at 22 m, where the first low beta magnet for the proton can be located.

These magnets can be built using standard superconducting and normal conducting magnet technology. The larger aperture of the third quadrupole magnet is needed to provide sufficient aperture for second, non-colliding, proton beam.

The colliding proton beam would pass off-centre through the lepton low beta triplet before entering the first magnet of the proton low-beta triplet at 22 m. The first magnet must ensure an integrated strength of 1564 T, the second lens requires 2070 T and

the third lens has an integrated gradient of 1058 T. The total length is about 45 m. Gradients in the order of 115 T/m are required and an aperture of 15 mm is to be provided. All quadrupole magnets are assumed to have a cold beam pipe and cold iron to provide flux return.

The first of these magnets is a septum half quadrupole as in the case of the HERA interaction region. The width of the septum is 12mm. The pole tip field is 2.79 T. The mirror-yoke is made of high quality magnetic steel. The large return yoke of the quadrupole magnets of the second proton low-beta lens accommodates a warm, cooled beam pipe for the lepton beam. The separation at the third group of magnets of the proton low beta triplet is sufficiently large, so the lepton can pass outside the cryostat.

After the low-beta triplet of the proton beam, the lepton beam is deflected by 5 mrad vertically using two 10m long dipoles which provide kicks of 1 mrad and 4 mrad respectively. At the end of the straight section, the lepton beam is about 80 cm above the proton beam axis. The proton beams orbits diverge to 80 cm separation. After the vertical deflection of the lepton beam, the protons are matched to their arc trajectory with three ten meter long superconducting dipole magnets.

The non-colliding proton beam is assumed to cross the colliding proton beam at the IP with an angle of 3.5 mrad and a sufficiently vertical separation. It is assumed to bypass the proton low-beta triplet. No attempts have been made to produce a layout of the lattice for this beam in the IR because it seems non-problematic.

This arrangement allows for a beta function of the lepton beam at the IP of β^*= 55 mm in both planes. The peak values of the vertical and horizontal lepton beta functions amount to 906 m and 269 m. The critical chromaticity contributions from the IR are quite modest with values of ξ_{xIR}= -18 and ξ_{yIR}= -38, which is about 25% of the contributions of the arc. Correction of this chromaticity is not expected to result in any significant reduction of dynamic aperture. The horizontal and vertical peak beta functions of the proton beam are 2668 m and 2637 m and so are considerably smaller than at the proton-proton interaction points and are assumed to be non-problematic. The IR chromaticity contributions of the proton beam are ξ_{pir}= -8.

The low beta quadrupole lenses provide sufficient aperture of at least 13.5 times the RMS beam size in the case of protons and at least 20 times the RMS beam size in the case of leptons. According to experience at HERA [87], this would be sufficient for avoiding beam lifetime reductions or poor backgrounds.

The interaction region is sketched in Fig. 23 and Fig. 24. The lattice functions are plotted in Fig. 25. The Interaction region parameters are shown in Table 5.

The crossing angle of $\theta_c = 0.5$ mrad would reduce the luminosity by a factor of 1.28. One can recover from this reduction and can avoid any detrimental effects from the finite crossing angle if the proton beam is tilted around a vertical axis by $\theta_c/2$. This can be accomplished by RF resonators with a transverse deflecting field, so-called crab cavities. In order to obtain an almost linear kick with the distance from the centre of the proton bunch over the entire length of the bunch (σ_p= 75 mm is the RMS proton

Table 5: Parameters of the high luminosity interaction region for the LHeC

Interaction region parameters			
property	**unit**	**leptons**	**protons**
Horizontal Beta function at IP	cm	5.5	180
Vertical beta function at IP	cm	5.5	50
Horizontal IR Chromaticity		-20	-15.4
Vertical IR chromaticity		-38	-13.8
Maximum horizontal Beta	m	268.7	2279
Maximum vertical Beta	m	909.2	2161
Minimum of available Aperture	σ_x	16	13.5
Low beta quadrupole gradient	T/m	93.3	115
Separation dipole field	T	0.033	-
Sychrotron Radiation Power	kW	18	-
Low beta quadrupole length	m	.96/2.43/1.14	16.5/18.6/11
Low beta quadrupole apertures	mm	30/40/50	12/15/15
Distance of first quadruple from IP	m	1.2	13.74
Detector Acceptance Polar Angle	degree	9.4	
Crossing Angle	mrad	0.5	

bunch length), the RF wave length has to be much larger than the bunch length. An RF frequency of 500 MHz fulfils this requirement (the nonlinearity at one times σ_p amounts to 9 %). Assuming beta functions of 1000 m at the properly placed crab cavities, the required transverse kick at one times σ_p from the centre is $\kappa = 0.59\mu$rad.

The RF phase angle corresponding to one times σ_p is 42°. This means that the RF structure has to provide an integrated peak field *of* $U_{crab} = \kappa E_p$ =6.2 MV. With a gradient of G_{crab} =3.4 MV/m, the two crab cavities systems around the IP must have an active length of 1.8m each. This could be accomplished by a 6-cell resonator. A four metre long superconducting 500 MHz RF structure is not expected to affect the LHC impedance budget considerably if the higher order modes are damped below a Q_{HOM} of 1000. Shorting of the resonators during p-injection and ramping may be required.

The two crab cavities can be installed in the IR at the point of maximum separation of the proton orbits between 120 m and 140 m distance from the IR. The horizontal phase advance at 120 m from the IP amounts to 25.6°. Thus a 3^{rd} resonator may be needed to provide exact closure of the crab-orbit bump. In order to avoid blow-up of the proton beam, the tolerances on the RF system and the required precision of the field amplitudes in the presence of high beam loading are very large. No attempt has been undertaken so far to specify an RF design for the crab-system.

For the low x, low Q^2 part of the physics programme, the detector needs acceptance within angles of 1 to 10° with respect to the detector axis. This cannot be provided

by the high luminosity IR as presented here. Since this part of the physics programme needs substantially less luminosity ($\sim$ one order of magnitude), the low beta magnets can be placed further away from the IP (by 3m), the beta function at the IP increased by a factor of 4 and a larger crossing angle can be tolerated. The low beta quadrupole triplet for the lepton beam needs a larger aperture to accommodate all the beams. No further effort was made with the low x IR configuration, which is not expected to represent a design challenge.

6.6 Synchrotron Radiation

The synchrotron radiation produced by the beam separation magnets, by misalignment of quadrupole magnets, and by closed orbit distortions in the IR, must be minimized by using beam-based alignment, by careful orbit control and by an effective collimation system. These issues have been discussed in the preparation and the commissioning of the HERA luminosity upgrade [92, 93]. The details will not be discussed here but it is important to notice that the synchrotron radiation produced in the proposed IR is somewhat less critical than in the case of HERA.

The soft bending field with a bend radius of ρ_{ir} =7105 m produces a radiation of 18 kW and a critical energy of 107 keV which is transported within a fan of 2.5 mrad horizontal opening angle and a vertical RMS thickness of $\approx$2 mm. The narrow opening angle of the fan is due to the anti-symmetric arrangement of the IR. Due to the crossing angle in the IP, the whole synchrotron radiation fan is tilted by 0.5 mrad away from the proton beam. Therefore, the high power synchrotron radiation does not penetrate the cold low-beta quadrupole magnets of the proton beam. Fig. 26 shows the distribution of synchrotron radiation in the IR.

The radiation is stopped at the 1m long absorber placed at 21 m from the IP before the first proton low-beta quadrupole. The linear power density reaches maximum values of 4.5 kW/cm (Fig. 27). The absorbing surface is tilted by (π/2-5mrad) so that the surface power density is reduced to approximately 110 W/mm^2. A corresponding collimator exists at HERA [93, 95]. It absorbs about 3 to 4 kW of radiation with a power density of 40 W/mm^2. The absorber presented here (Fig. 28) is a realistic extrapolation of the HERA absorber. A sketch of a possible absorber for LHeC is shown in Fig. 28. A second absorber is needed between the first and the second low beta quadrupole of the protons. According to HERA experience [94] this collimation system should be adequate for both elimination of experimental background and protection of accelerator components.

6.7 Magnetic Elements of the Interaction Region

The superconducting low beta quadrupoles for the electron beam can be built using standard superconducting technology. The first two low beta quadrupoles for the

protons are more challenging, because the lepton beam pipe has to pass through the cryostat of these magnets.

The first lens is a septum quadrupole laid out as a superconducting half quadrupole. The radius of the half aperture is 30 mm which provides a 15 mm aperture for the beam. The left side half of the magnets looks like a standard superconducting quadrupole (Fig. 29). The other half consists of magnetic iron with a gap for the lepton beam. The achieved gradient is 93 T/m. The magnetic mirror plate works well up to a magnetic induction of 2.79 near the coil. The magnet has a reasonable field quality and has no field in the gap for the lepton beam. This has been confirmed by magnetic field calculation using the code Opera-2D [96]. Figures 29, 30 and 31 show a cross section with the conceptual layout and the results of the field calculation. A possible issue with this magnet is the mechanical stability of the coil.

At the second proton low beta quadrupole which needs the full horizontal aperture, the two beams are separated by 85mm so that the lepton beam pipe can pass outside the regular coil through the flux return yoke. This magnet needs a wide flux return. The coil is a standard superconducting quadrupole coil with an aperture of 30mm.

6.8 Beam-Beam Effects and Luminosity

In the following, the luminosity will be recalculated from the design parameters. The large bunch length of the proton beam of 7.55 cm will cause a luminosity reduction since it enhances the effective beam size of the protons experienced by the electron beam. The effect of the short lepton bunch length can be neglected and the so-called hour glass luminosity reduction factor is

$$R = \frac{2 \cdot \beta_{yp}\beta_{ye}}{\sqrt{\pi}\sigma_p\sqrt{\beta_{yp}^2+\beta_{ye}^2}} \cdot \exp\left(2 \cdot \frac{\beta_{yp}\beta_{ye}}{\sigma_p\sqrt{\beta_{yp}^2+\beta_{ye}^2}}\right) \cdot K_0\left(\left(\frac{\beta_{yp}\beta_{ye}}{\sigma_p\sqrt{\beta_{yp}^2+\beta_{ye}^2}}\right)^2\right) = 0.92 \tag{14}$$

The crossing angle should not reduce the luminosity if it is properly compensated by the crab-tilt of the proton bunches.

Another effect which influences the luminosity is the so-called dynamic beta, the distortions of the beta functions in the core of the beam by the beam-beam interaction. This distortion decreases the lepton beta functions at the IP in the electron-proton case if the tunes are above the integer and below the half integer resonance

$$\frac{\Delta\beta_{x,y}}{\beta_{x,y}} = \frac{r_0 \cdot N_p \cdot \beta_{x,y} \cdot \cot(2 \cdot \pi \cdot Q_{x,y})}{\gamma_e \cdot \sigma_{x,y}^p \cdot (\sigma_x^p + \sigma_y^p)}. \tag{15}$$

This does not affect the beam tails and has no influence on the aperture need of the beam. It does affect, however, the beam matching and the chromaticity. Dynamic focusing can therefore not be used to increase the luminosity without taking it into account the considerations chromaticity limitations as discussed before. The dynamic

beta depends strongly on the choice of the tunes. For electron-proton interactions and for the tunes above the integer and below the half integer resonance, one obtains an additional focusing. For HERAe-like tunes Q_{xe}= 0.10 and Q_{ye} = 0.11 one obtains a small reduction of the electron beta functions from β_{ex}= 5 cm to β_{ex}= 3.77 cm, and from βey =5cm to β_{ye} = 4.44 cm. Note that for positron, the tunes should be taken below the integer resonance.

The beam-beam tune shift values which result from the parameters are

$$\Delta\nu_x^p = \frac{r_p N_e \beta_{xp}}{2\pi\gamma_p\sigma_{xe}(\sigma_{xe}+\sigma_{xe})} = 1.28\cdot 10^{-3} \tag{16}$$

$$\Delta\nu_y^p = \frac{r_p N_e \beta_{yp}}{2\pi\gamma_p\sigma_{ye}(\sigma_{xe}+\sigma_{xe})} = 2.69\cdot 10^{-3} \tag{17}$$

$$\Delta\nu_x^e = \frac{r_0 N_p \beta_{ye}}{2\pi\gamma_e\sigma_{xp}(\sigma_{xp}+\sigma_{xp})} = 21\cdot 10^{-3} \tag{18}$$

$$\Delta\nu_y^e = \frac{r_0 N_p \beta_{ye}}{2\pi\gamma_e\sigma_{xp}(\sigma_{xp}+\sigma_{xp})} = 39\cdot 10^{-3}. \tag{19}$$

These tune shift values are well within the range of HERA operational parameters and given the large beam energy of 70GeV and the short damping time, they may be considered a safe choice.

The long-range beam-beam tune shift parameters $\Delta\nu_x^{par}$, $\Delta\nu_y^{par}$ of the lepton beam at the parasitic crossings are given by [97]

$$\Delta\nu_x^{par} = \frac{N_p r_0 \beta_x^{par}}{2\pi\gamma_e\Delta x^2} \tag{20}$$

$$\Delta\nu_y^{par} = \frac{-N_p r_0 \beta_y^{par}}{2\pi\gamma_e\Delta x^2} \tag{21}$$

($\beta_{x,y}^{par}$ are the beta functions and Δx is the horizontal beam separation at the parasitic crossing; the vertical beam separation is zero). The corresponding values for the first three parasitic crossings are quite large for a bunch spacing of 25ns (see Tab. 6 which summarizes the evaluation of these formulae, adding the values from the first three parasitic crossings from both sides of the IP). For a bunch spacing of 75 ns the long range beam-beam parameters are sufficiently small. A larger crossing angle reduces the long range beam-beam effects. However, even a doubling of the crossing angle from 0.5 mrad to 1mrad does not relax the long-range beam-beam sufficiently. The coherent beam-beam footprint would increase the beam-beam tune spread over the whole beam to 0.07 in the vertical plane (including the bunches near the abort gap). This quite large tune footprint would fit however in between synchrotron sideband resonances due to large longitudinal tune of Q_s= 0.15. The operational experience with long-range beam-beam effects in LEP [98] (at four instead of at one interaction point) indicates, that even with tune shift values corresponding to a 75ns bunch spacing, one has to expect problems mainly due to beam-beam orbit effects. The conclusion from this analysis is that the long-range beam-beam forces are quite large for a bunch spacing of

Table 6: Parasitic beam-beam tune shifts of the lepton beam

Parasitic Beam-Beam Tune shifts of the Lepton Beam				
Bunch spacing	Crossing angle	Horizontal Separation	horizontal parasitic beam-beam tune shift	vertical parasitic beam-beam tune shift
[ns]	[mrad]	[mm]		
25	0.5	2.78	0.0129	-0.0353
50	0.5	7.63	0.0088	-0.0211
75	0.5	14.47	0.0005	-0.0042
25	1	2.78	0.0053	-0.0199
50	1	7.63	0.0020	-0.0098
75	1	20.1	0.0003	-0.0022

25ns. Without further study, it cannot be excluded, that a larger bunch spacing might be necessary.

Taking these effects into account the luminosity for I_e= 74mA, N_p= 1.68 10^{11}, γ_p = 7460, ε_p= 0.5 nm, ε_{xe}= 25 nm, ε_{ye} = 5 nm and $R = 0.89$ amounts to

$$L = \frac{I_e \cdot N_p \cdot \gamma_p \cdot R}{4 \cdot \pi \cdot e \cdot \sqrt{\varepsilon_p \beta_{xp} + \varepsilon_{ye} \beta_{ye}} \cdot \sqrt{\varepsilon_p \beta_{yp} + \varepsilon_{ye} \beta_{ye}}} = 1.04 \cdot 10^{33} cm^{-2} s^{-1} \quad , \qquad (22)$$

according to the design goal.

7 Summary

The physics and the design of a Large Hadron Electron Collider (LHeC) are sketched. It is illustrated that a unique and important programme of physics is possible with a 70 GeV electron/positron beam in collision with the 7 TeV LHC proton (and ion) beam at a luminosity of $10^{33}\mathrm{cm}^{-2}\mathrm{s}^{-1}$.

Experiments at such a collider probe electron-quark and positron-quark physics in an unparalleled manner, thereby enabling a substantial extension of the discovery potential at the LHC and making possible measurements of a precision characteristic of lepton-hadron measurements. Highlights include

- Observation and precision measurement of new physics in the lepton-quark spectrum at the TeV scale, which could reveal unexpected and new leptoquark phenomena. The LHeC will provide precision measurements which are important to the interpretation and quantification of this new physics.

- Discovery and precision measurement of new physics in proton structure at very low Bjorken-x which will be crucial to the development of our understanding of QCD in the high parton density, low coupling limit, and thereby the phase equilibria of chromodynamics in a variety of hadronic systems at the TeV energy scale.

- A new level of precision measurements and precision tests of the validity of QCD at a new distance scale, corresponding to substructure dimensions of 10^{-19} m, which promise to have a direct bearing on the overall consistency of the Standard Model and its underlying physics as one moves towards the unification scale.

- Measurements which will make possible the determination of parton distribution functions of nucleons and nuclei over a hitherto inaccessible kinematic range in probe scale (Q^2) and longitudinal momentum (Bjorken-x), and which are essential if the sensitivity at the LHC to new and rare physics in both pp and ep physics is to be optimal.

A conceptual design of a high luminosity Large Hadron Electron Collider, the LHeC, is presented. The approach takes advantage of developments in technology which are now well advanced, and which are necessary for future electron/positron linear accelerators, to achieve an electron/positron storage ring of for example 70 GeV energy in the LHC tunnel. It is shown how, with the careful design of the RF structure and the interaction region, it is possible to achieve a luminosity of $10^{33}\,\mathrm{cm}^{-2}\mathrm{s}^{-1}$ in collisions with one of the LHC hadron beams. The solution is based on 25 ns bunch spacing with a small crossing angle of 0.5 mrad which requires crab-crossing for the proton beam. The concept is aimed at the simultaneous operation of LHC and LHeC and first considerations of how this can be achieved are stated. Wherever possible, realistic constraints are included based on past operation of electron storage rings and on the operation of the HERA electron and proton storage rings at DESY Hamburg.

Further work is needed to address a number of issues which have yet to be resolved concerning the feasibility of such a concept. Nevertheless, to date it appears not unreasonable to continue to contemplate a major and important ep physics programme at the TeV scale as part of the physics programme of the LHC.

Acknowledgement

The authors wish to thank G. Altarelli, W. Bartel, J. Blümlein, S. Brodsky, A. Bruell, A. Caldwell, A. DeRoeck, M. Diehl, J. Ellis, R. Engel, J. Engelen, H. Jung, J. Feltesse, S. Forte, A. Glazov, T. Greenshaw, R. Heuer, E. Kabuss, T. Lastovicka, M. Mangano, S. Myers, C. Niebuhr, D. Pitzl, B. Reisert, R. Rueckl, D. Schlatter, S. Schlenstedt, M. Seidel, R. Schmitt, U. Stoesslein, M. Strikman, R. E. Taylor, W. K. Tung, and A. Zarnecki for interesting discussions and providing valuable information.

The authors have worked for two decades at the world's first high energy collider of different particle species, HERA at DESY. It would be inappropriate not to record our thanks also to many colleagues, too numerous to name here, with whom we have worked throughout this time at HERA and who have developed the physics and the techniques for experimentation at such a collider, on which much of the plans sketched here relies.

References

[1] R. P. Feynman, Lepton Hadron Interactions, New York 1972.

[2] R. P. Feynman, Phys. Rev. Lett. **23** (1969) 1415;
J. D. Bjorken, Phys. Rev. **D1** (1970) 1376;
J. D. Bjorken and E. A. Paschos, Phys. Rev. **185** (1969) 1975.

[3] J. I. Friedman, H. W. Kendall, R. E. Taylor, Nobel Prize lectures 1990.

[4] D. Gross, H. Politzer, F. Wilczek, Nobel Prize lectures 2004.

[5] R. Brinkmann, Snowmass Workshop 2001, Proceedings;
F. Willeke, Snowmass Workshop 2001, Proceedings;
see also the THERA Book [9].

[6] D. Schulte and F. Zimmermann, "QCD Explorer based on LHC and CLIC-1", CERN AB-2004-079, CLIC Note 608;
see also L. Gladilin et al., hep-ph/0504008.

[7] J. Feltesse, Talk at the LHC Workshop, Aachen 1990, CERN 90-10 (1990), Proceedings Vol.1 p.219, eds. C. Jarlskog and D. Rein.

[8] R. Rückl, Talk at the LHC Workshop, Aachen 1990, CERN 90-10 (1990), Proceedings Vol.1 p.229, eds. C. Jarlskog and D. Rein.

[9] The THERA Book, *ep* Scattering at $\sqrt{s} \sim 1\,\text{TeV}$, DESY 01-123F, eds. U. Katz, M. Klein, A. Levy and S. Schlenstedt.

[10] A. Verdier, Talk at the LHC Workshop, Aachen 1990, CERN 90-10 (1990), Proceedings Vol.1 p.820, eds. C. Jarlskog and D. Rein.

[11] W. Bartel, ibid, p.824.

[12] E. Keil, LHC Project Report, 93(1997).

[13] CERN Council Strategy Group,
http://council-strategygroup.web.cern.ch/council-strategygroup/

[14] A. Zarnecki in [9] and private communication.

[15] A. Belyaev, C. Leroy, R. Mehdiyev and A. Pukhov, JHEP **0509** (2005) 005 [hep-ph/0502067].

[16] P. Taxil, E. Tugcu and J.M. Virey, Eur. Phys. J. **C14** (2000) 165 [hep-ph/9912272].

[17] A. Djouadi et al., Z. Phys. **C46** (1990) 679.

[18] W. Buchmüller, R. Rückl and D. Wyler, Phys. Lett. **B191** (1987) 442. *Erratum* Phys. Lett. **B448** (1999) 320.

[19] F. Wilczek, Int. J. Mod. Phys. **A 16** (2001) 1653 [hep-ph/0101187].

[20] V.N. Gribov, E.M. Levin and M.G. Ryskin, Phys. Rep. **100** (1983) 1.
A. Mueller, hep-ph/0501012 and references therein.

[21] E. Iancu, A. Leonidov and L. McLerran, Nucl. Phys. **A692** (2001) 583;
For a review and references see: E. Iancu and M. Venugopalan, Review for QGP3, Eds. R. C. Hwa and X.-N. Wang, World Scientific [hep-ph/0303204].

[22] E. A. Kuraev, L. N. Lipatov and V. S. Fadin, Sov. Phys. JETP **44** (1976) 443 [Zh. Eksp. Teor. Fiz. **71** (1976) 840];
E. A. Kuraev, L. N. Lipatov and V. S. Fadin, Sov. Phys. JETP **45** (1977) 199 [Zh. Eksp. Teor. Fiz. **72** (1977) 377];
I. I. Balitsky and L. N. Lipatov, Sov. J. Nucl. Phys. **28** (1978) 822 [Yad. Fiz. **28** (1978) 1597].

[23] M. Ciafaloni, Nucl. Phys. B **296** (1988) 49;
S. Catani, F. Fiorani and G. Marchesini, Phys. Lett. B **234** (1990) 339;
S. Catani, F. Fiorani and G. Marchesini, Nucl. Phys. B **336** (1990) 18;
G. Marchesini, Nucl. Phys. B **445** (1995) 49 [hep-ph/9412327].

[24] I. Balitsky, Nucl. Phys. **B463** (1996) 99 [hep-ph/0101042];
Yu. V. Kovchegov, Phys. Rev. **D60** (1999) 034008; *ibid.* **D61** (2000) 074018.

[25] V. N. Gribov and L. N. Lipatov, Sov. J. Nucl. Phys. **15** (1972) 675 [Yad. Fiz. **15** (1972) 1218];
V. N. Gribov and L. N. Lipatov, Sov. J. Nucl. Phys. **15** (1972) 438 [Yad. Fiz. **15** (1972) 781];
L. N. Lipatov, Sov. J. Nucl. Phys. **20** (1975) 94 [Yad. Fiz. **20** (1974) 181];
G. Altarelli and G. Parisi, Nucl. Phys. B **126** (1977) 298;
Y. L. Dokshitzer, Sov. Phys. JETP **46** (1977) 641 [Zh. Eksp. Teor. Fiz. **73** (1977) 1216].

[26] G. Altarelli, R.D. Ball and S. Forte, hep-ph/0512237.

[27] S. Moch, J. Vermaseren and A. Vogt, Nucl. Phys. **688** (2004) 101 and **691** (2004) 129 and Nucl. Phys. B **724** (2005) 3 [hep-ph/0504242].

[28] A.H. Müller, Nucl. Phys. **B415** (1994) 373; *ibid.* **B437** (1995) 107;
A.H. Müller and B. Patel, Nucl. Phys. **B425** (1994) 471.

[29] K. Golec-Biernat, M. Wüsthoff, Phys. Rev. **D59** (1999) 014017;
K. Golec-Biernat, M. Wüsthoff, Phys. Rev. **D59** (1999) 114023;
J. Bartels, K. Golec-Biernat, H. Kowalski, Phys. Rev. **D66** (2002) 014001.

[30] J. Bartels, Eur. Phys. J. **C 43** (2005) 3.

[31] E. Gotsman, E. Levin, U. Maor, E. Naftali, hep-ph/0504040.

[32] H1 Collab., A. Aktas et al., Accepted by Eur Phys J, hep-ex/0508055;
ZEUS Collab., S. Chekanov et al., Phys. Lett. **B632** (2006) 13 [hep-ex/0502029].

[33] H1 Collab., A. Aktas et al., Eur. Phys. J. **C33** (2004) 477 [hep-ex/0310019].

[34] ALICE Collab., F Carminati et al., J. Phys. G: Nucl. Part. Phys. **30** (2004) 1517.

[35] V. Gribov, Sov. Phys. JETP **30** (1970) 709.

[36] For a review and references see: R. Engel, astro-ph/0504358.

[37] S. Brodsky et al., Phys.Rev. **D65** (2002) 114025. WO?

[38] M. Klein and T. Riemann, Z. Phys. C **24** (1984) 151.

[39] D. Mason, NuTeV Collaboration, hep-ex/0405037.
S. Kretzer and F. I. Olness, AIP Conf. Proc. **792** (2005) 843 [hep-ph/0508216].

[40] M. Dittmar, F. Pauss and D. Zurcher, Phys. Rev. **D56** (1997) 7284 [hep-ex/9705004]; A. Cooper-Sarkar et al., Summary of Structure Function Working Group [44].

[41] W.J. Stirling, Talk at the Binn Workshop on Physics at the LHC, October 2003.

[42] A. D. Martin, R. G. Roberts, W. J. Stirling and R. S. Thorne, Eur. Phys. J. C **35** (2004) 325 [arXiv:hep-ph/0308087].
A. Cooper-Sarkar et al., Summary of Structure Function Working Group [44].

[43] A. Martin, M. Ryskin, G. Watt, Eur.Phys.J. **C37** (2004) 285.

[44] Proceedings of the "HERA and the LHC Workshop", CERN-2005-014, DESY-PROC-2005-001, Eds. A. De Roeck and H. Jung.

[45] H1 Collab., A. Aktas et al., Eur. Phys. J. **C40** (2005) 349 [hep-ex/0411046];
H1 Collab., A. Aktas et al., Eur. Phys. J. **C45** (2006) 23 [hep-ex/0507081].

[46] B.C. Allanach et al., hep-ph/0403133.

[47] For a recent calculation see: Q. Mason et al, hep-lat/0503005.

[48] W. van Neerven, in [9].

[49] C. Glasman, hep-ex/0506035.

[50] H1 Collaboration, C. Adloff et al., Eur. Phys. J. **C21** (2001) 33 [hep-ex/0012053].

[51] ZEUS Collaboration, S. Chekanov et al., Eur. Phys. J. C **42** (2005) 1 [hep-ph/0503274].

[52] Wu Ki Tung, private communication.

[53] A. D. Martin, R. G. Roberts, W. J. Stirling and R. S. Thorne, hep-ph/0307262.

[54] V. Khoze, A. Martin, M. Ryskin, Eur. Phys. J **C23** (2002), 311;
A. de Roeck et al., Eur. Phys. J **C25** (2002) 391.

[55] ZEUS Collaboration, M. Derrick *et al.*, Phys. Lett. **B315** (1993) 481;
H1 Collaboration, T. Ahmed *et al.*, Nucl. Phys. **B429** (1994) 477.

[56] J. Collins, Phys. Rev. **D57** (1998) 3051 and erratum-ibid. **D61** (2000) 019902.

[57] See for example H1 Collaboration, C. Adloff *et al.*, Zeit. Phys. **C76** (1997) 613.

[58] For a review see J. Collins et al., in[44].

[59] M. Krawczyk and M. Zembrzuski in [9].

[60] D. Mueller et al., Fortschritte der Physik **42** (1994) 101 [hep-ph/9812448];
For a review see M. Diehl, Phys. Rep. **388** (2003) 41.

[61] A.V. Belitsky and D. Müller, hep-ph/0206306.
For a review see: A.V. Belitsky and A.V. Radyushkin, hep-ph/0504030.

[62] S. V. Goloskokov and P. Kroll, Eur. Phys. J. C **42** (2005) 281 [hep-ph/0501242].

[63] M. Arneodo et al., hep-ph/9610423.

[64] T. Alexopoulos *et al.*, eD Scattering with H1, A Letter of Intent, DESY 03-194;
H. Abramowicz *et al.*, A New Experiment for HERA, MPP-2003-62;
F. Willeke and G. Hoffstaetter, Talks at the Workshop on the Future of DIS, Durham 2001, unpublished;
M. Klein and T. Greenshaw, J. Phys. G Nucl. Part. Phys. **28** (2002) 2505;
http://hep.ph.liv.ac.uk/∼green/HERA3/.

[65] L. Merminga and Yu. Derbenev, Contribution to CIPANP2003;
R. Ent, Report to NSAC Subcommittee, BNL, June 2004, http://nsac2004.bnl.gov/pres/ent.pdf.
"Electron-Ion Collider at CEBAF: New Insights and Conceptual Progress", Y. Derbenev, et al., Proc. EPAC 2004

[66] eRHIC homepage, http://www.phenix.bnl.gov/WWW/publish/abhay/
Zero-design-Report http://www.rhichome.bnl.gov/eRHIC/

[67] R. Milner, Report to NSAC Subcommittee, BNL, June 2004, eRHIC [66].

[68] For reviews and references see: M. Gyulassy and L. Mc Lerran, Nucl. Phys. **A 750** (2005) 30 [hep-ph/0405013];
A. Mueller and A.I. Soshi, hep-ph/0402193.

[69] L. Frankfurt and M. Strikman, Eur. Phys. ,J. **A5**(1999)293.

[70] L. Frankfurt, V. Guzey, M. McDermott and M. Strikman, hep-ph/0104154.
see also L. Frankfurt, M. Strikman and C. Weiss, Ann. Rev. Nucl. Sci. **55** (2005) 403.

[71] M. Strikman, private communication.

[72] S. Forte, private communication.

[73] M. Botje, M. Klein and C. Pascaud, HERA Workshop 1996, Proceedings Hamburg 1996, p. 33, eds. G. Ingelman, R. Klanner and A. De Roeck [hep-ph/9609489].

[74] A. Blondel and F. Jacquet, Proceedings of the Study of an *ep* Facility for Europe, ed. U. Amaldi, DESY (1979) 391.

[75] TOTEM Collaboration, V. Beradi et al., technical design report, CERN-LHCC-2004-002

[76] http://www.fp420.com/index.html;
FP420 : An R+D Proposal to Investigate the Feasibility of Installing Proton Tagging Detectors in the 420 m Region at LHC, M.G. Albrow et al., CERN-LHCC-2005-025;

[77] M. Tigner, B. Wiik and F. Willeke, An electron proton collider in the TeV range, in Proc. IEEE Particle Accelerator Conference, San Franscisco, p.2910 (1991)

[78] www.SLAP.web.cern.ch/slap/lhc-parameter.htm

[79] R. Brinkmann, F. Willeke: FIRST EXPERIENCE WITH COLLIDING ELECTRON PROTON BEAMS IN HERA, Prepared for 1993 IEEE Particle Accelerator Conference (PAC 93), Washington, DC, 17-20 May 1993. Particle accelerator, vol. 5* 3742-3744.

[80] S. Poulsen, CERN, Geneva, Switzerland: AN INDUSTRIAL CONTROL SYSTEM FOR THE SUPERVISION OF THE CERN ELECTRICAL DISTRIBUTION NETWORK, International Conference on Accelerator and Large Experimental Physics Control Systems, 1999, Trieste, Italy; http://cernenviro.web.cern.ch/CERNenviro/Pages/E/Themes/Electricity/Electricity.html

[81] M. Sands, The Physics of Electron Storage Rings, Lecture given at the Ravenna School for Accelerator Physics 1976, unpublished

[82] R. Brinkmann, F. Willeke, CHROMATIC CORRECTIONS AND DYNAMIC APERTURE IN THE HERA ELECTRON RING. 2. DESY 87/037, May 1987;
R. Brinkmann, F. Willeke: CHROMATIC CORRECTIONS AND DYNAMIC APERTURE IN THE HERA ELECTRON RING, in Novosibirsk 1986, Proceedings, High energy accelerators, vol. 1* 87-90 and Hamburg DESY - DESY M-86-10 (86.) 5-8.

[83] F. Willeke, Proceedings of the 2nd Advanced ICFA Beam Dynamics Workshop, Lugano,1988, p.164, CERN 88-04 (1988).

[84] G. Hoffstaetter, F. Willeke: ELECTRON DYNAMICS IN THE HERA LUMINOSITY UPGRADE LATTICE OF THE YEAR 2000, DESY-M-99-02U, Jun 1999. 3pp., prepared for IEEE Particle Accelerator Conference (PAC 99), New York, NY, 29 Mar - 2 Apr 1999, published in *New York 1999, Particle Accelerator, vol. 1* 407-409

[85] A. Verdier, Proceedings of the 2nd Advanced ICFA Beam Dynamics Workshop, Lugano, 1988, p.186ff, CERN 88-04 (1988)

[86] The LEP Design Report, Vol II, CERN-LEP, 84-01 (1984)

[87] M. Bieler et al., RECENT AND PAST EXPERIENCES WITH BEAM-BEAM EFFECTS AT HERA, SLAC-PUB-8203, Nov 1999, prepared for Workshop on Beam-Beam Effects in Large Hadron Colliders, Geneva, Switzerland, 12-16 Apr 1999 inGeneva 1999, Beam-beam effects in large hadron colliders* 12-19.

[88] M.G. Minty: HERA PERFORMANCE UPGRADE: ACHIEVEMENTS AND PLANS FOR THE FUTURE, EPAC-2004-TUXLH02, Jul 2004. 5pp, presented at the 9th European Particle Accelerator Conference (EPAC 2004), Lucerne, Switzerland, 5-9 Jul 2004

[89] O. Gröbner, Experience from the LEP Vacuum System, Proceedings of the Workshop an VLHC, ITT, (2001)

[90] S. Belomestnykh, P. Barnes, E. Chojnacki, R. Ehrlich, R. Geng, D. Hartill, R. Kaplan, J. Knobloch, E. Nordberg, H. Padamsee, S. Peck, P. Quigley, J. Reilley, D. Rubin, J. Sears, V. Veshcherevich: COMMISSIONING OF THE SUPERCONDUCTING RF CAVITIES FOR THE CESR LUMINOSITY UPGRADE, Proceedings of the 1999 Particle Accelerator Conference, New York, 1999

[91] I.Ben-Zvi, Review of various approaches to address high currents in superconducting linacs, 12th International workshop on RF Superconductivity, Cornell July 2005 (2005)

[92] U. Schneekloth (ed), The HERA Luminosity Upgrade, DESY-HERA (1998)

[93] M. Seidel, HERA LUMINOSITY UPGRADE, DESY-M-99-02ZB, Jun 1999. 3pp. Prepared for IEEE Particle Accelerator Conference (PAC 99), New York, NY, 29 Mar - 2 Apr 1999, Published in *New York 1999, Particle Accelerator, vol. 1* 34.

[94] M. Bieler, E. Lohrmann, A. Meseck, G. Nawrath, M. Seidel, F. Willeke: DESIGN OF A HIGH POWER SYNCHROTRON RADIATION ABSORBER FOR HERA, DESY-M-99-02I, Jun 1999. 3pp. ,prepared for IEEE Particle Accelerator Conference (PAC 99), New York, NY, 29 Mar - 2 Apr 1999, Published in *New York 1999, Particle Accelerator, vol. 1* 554.

[95] M. Seidel, M. Hoffmann, VACUUM INDUCED BACKGROUNDS IN THE NEW HERA INTERACTION REGIONS, EPAC-2004-MOPLT045, DESY-M-04-03ZA, Oct 2004. 3pp. , Prepared for 9th European Particle Accelerator Conference (EPAC 2004), Lucerne, Switzerland, 5-9 Jul 2004.

[96] http://www.vectorfields.com/content/view/20/43/

[97] J. Jowett, in Handbook of Accelerator Physics and Engineering, A. Chao, M. Tigner, eds, World Scientific, Singapore (1999)

[98] W. Herr, EXPERIENCE WITH BEAM-BEAM EFFECTS, Nov 1999, prepared for Workshop on Beam-Beam Effects in Large Hadron Colliders, Geneva, Switzerland, April 1999, Beam-beam effects in large hadron colliders* 12-19.

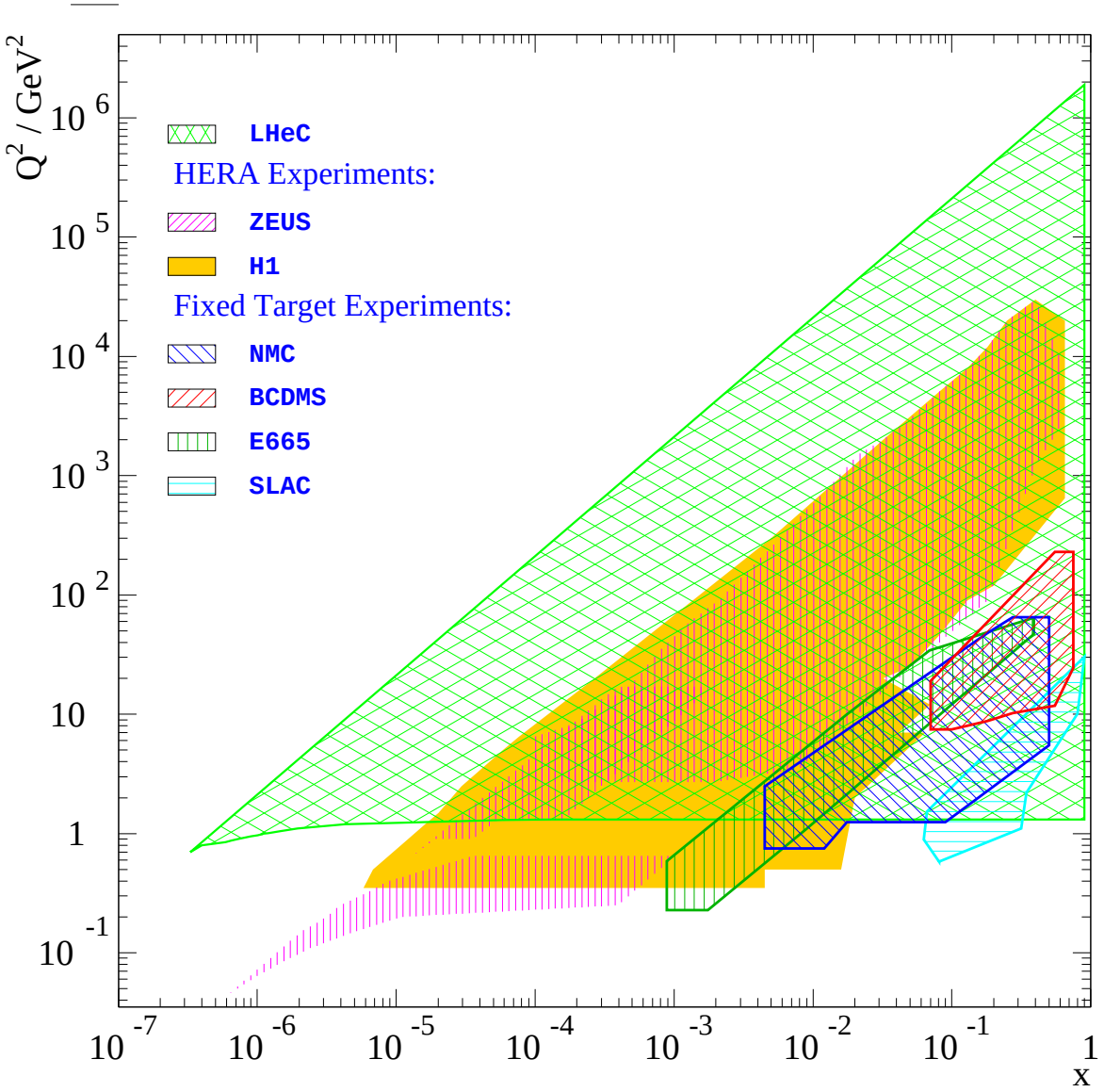

Figure 1: Kinematic regions in Bjorken x and momentum transfers Q^2 covered by fixed target unpolarised lepton-proton scattering experiments, the H1 and ZEUS experiments at HERA and the proposed electron-proton collider LHeC.

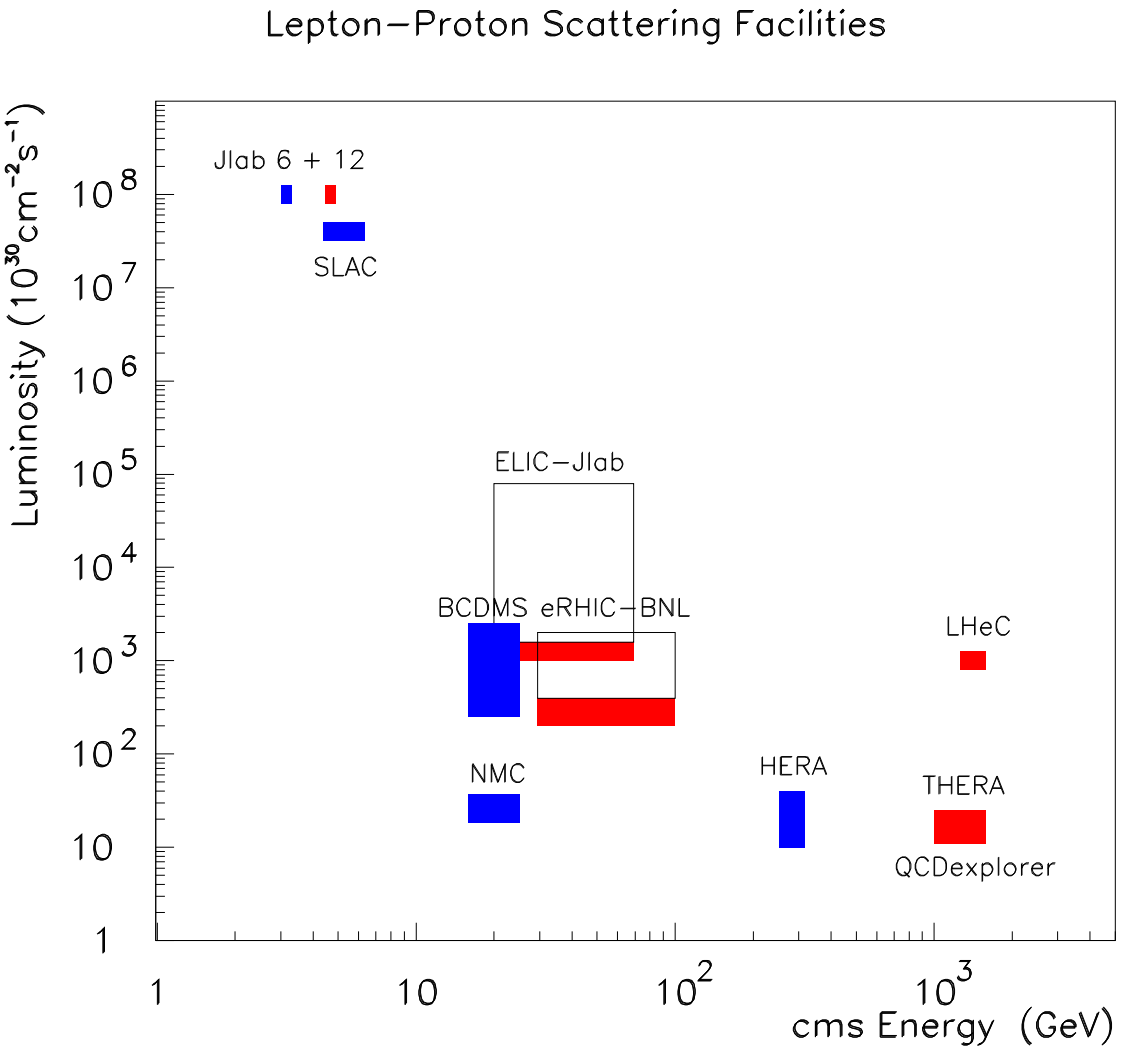

Figure 2: Summary of existing (dark, blue boxes) and proposed (grey, red boxes) facilities for unpolarised lepton-proton deep-inelastic scattering investigations in terms of the luminosity and cms energy. The Jlab fixed target programme is directed to high statistics physics at low Q^2 and very large x. The SLAC box indicates the luminosity of the classic ep experiment at the 2 mile linear accelerator. BCDMS and NMC have provided the most accurate DIS muon-proton structure function data using 30 m and 3 m long unpolarised hydrogen targets, respectively. The reach of largest luminosities at eRHIC and ELIC (hollow boxes), desirable for polarised ep physics, is related to the application of energy recovery linac techniques. HERA has reached peak luminosities of up to $4 \cdot 10^{31}\text{cm}^{-2}\text{s}^{-1}$ with a luminosity upgrade. The linac-ring accelerator designs of THERA (TESLA/ILC-HERA) and the QCD explorer (CLIC-LHC) hardly provide luminosity much above $10^{31}\text{cm}^{-2}\text{s}^{-1}$. The LHeC is designed for the highest energy at the largest luminosity.

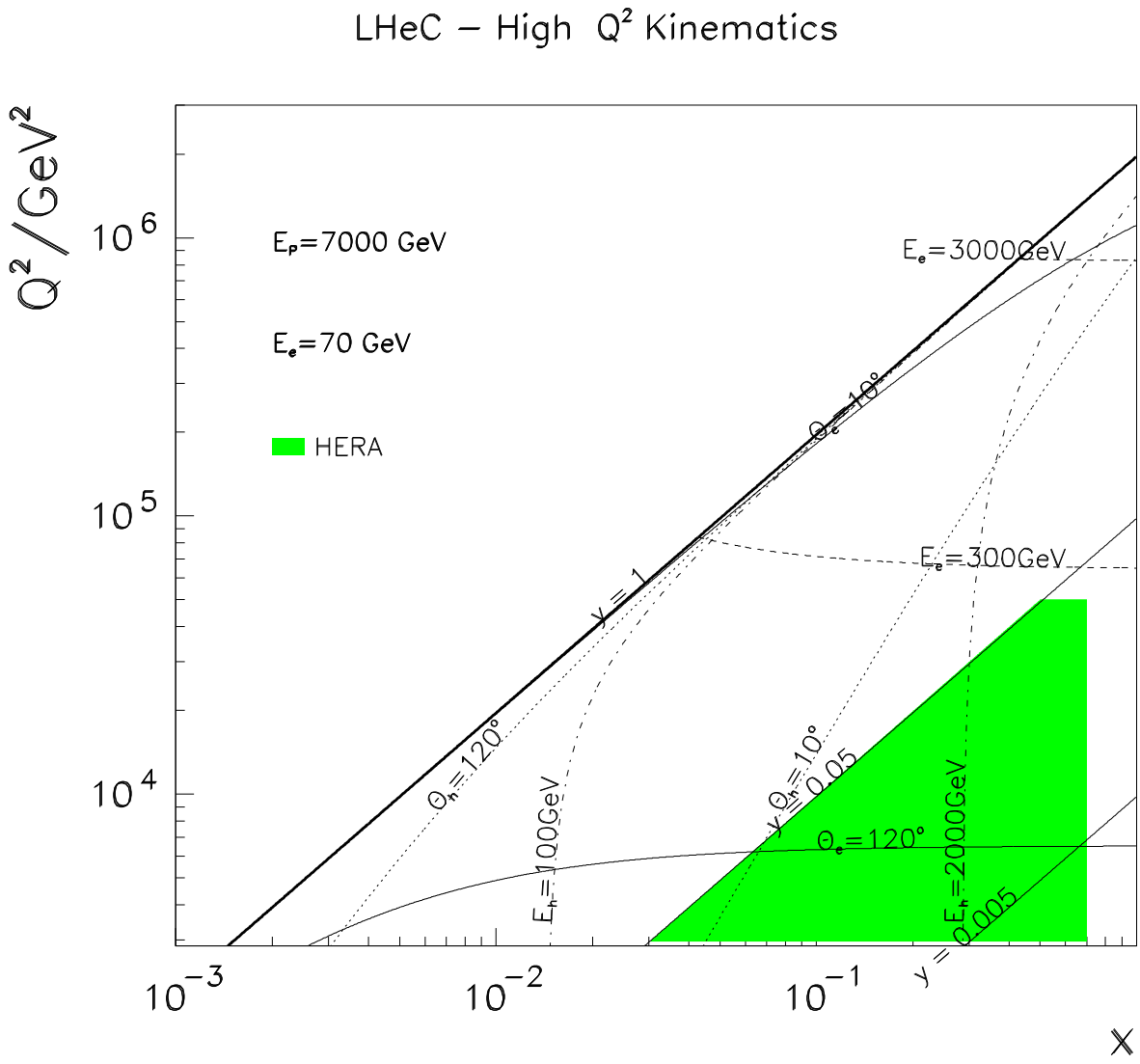

Figure 3: Kinematics of ep scattering at the LHeC at high Q^2. The shaded area illustrates the region of kinematic coverage in NC scattering at HERA. In ep scattering electron-quark resonances can be formed with mass $M = \sqrt{xs}$. Due to luminosity and energy range, the search limit at HERA has been at about 290 GeV while the LHeC extends to large M values of about 1300 GeV.

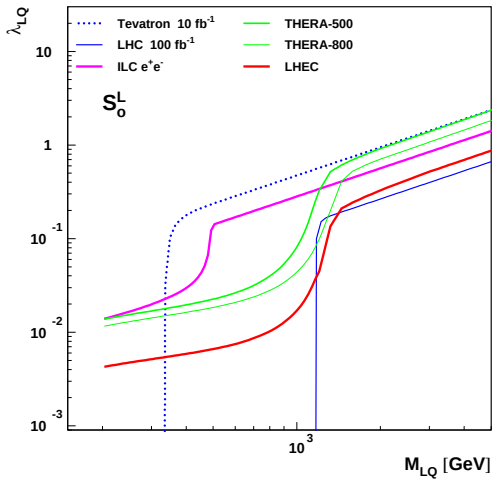

Figure 4: Mass-dependent upper bounds on the LQ coupling λ as expected at LHeC for a luminosity of 10 fb^{-1} (full red curve) and at the LHC for 100 fb^{-1} (full blue curve) [14]. These are shown for an example scalar LQ coupling to $e^- u$.

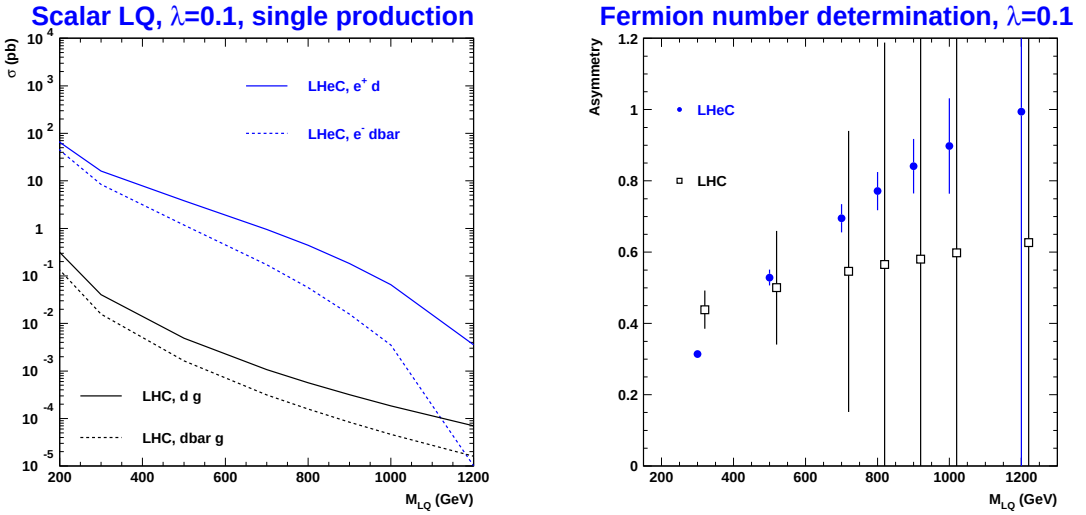

Figure 5: (Left) Single LQ production cross section at the LHeC (top) and LHC (bottom), for a scalar LQ coupling to $e^+ d$ and a coupling $\lambda = 0.1$; (Right) Asymmetries which would determine the fermion number of such a LQ, the sign of the asymmetry being the relevant quantity. An integrated luminosity of 100 fb^{-1} (10 fb^{-1} per lepton charge) has been assumed for the LHC (LHeC).

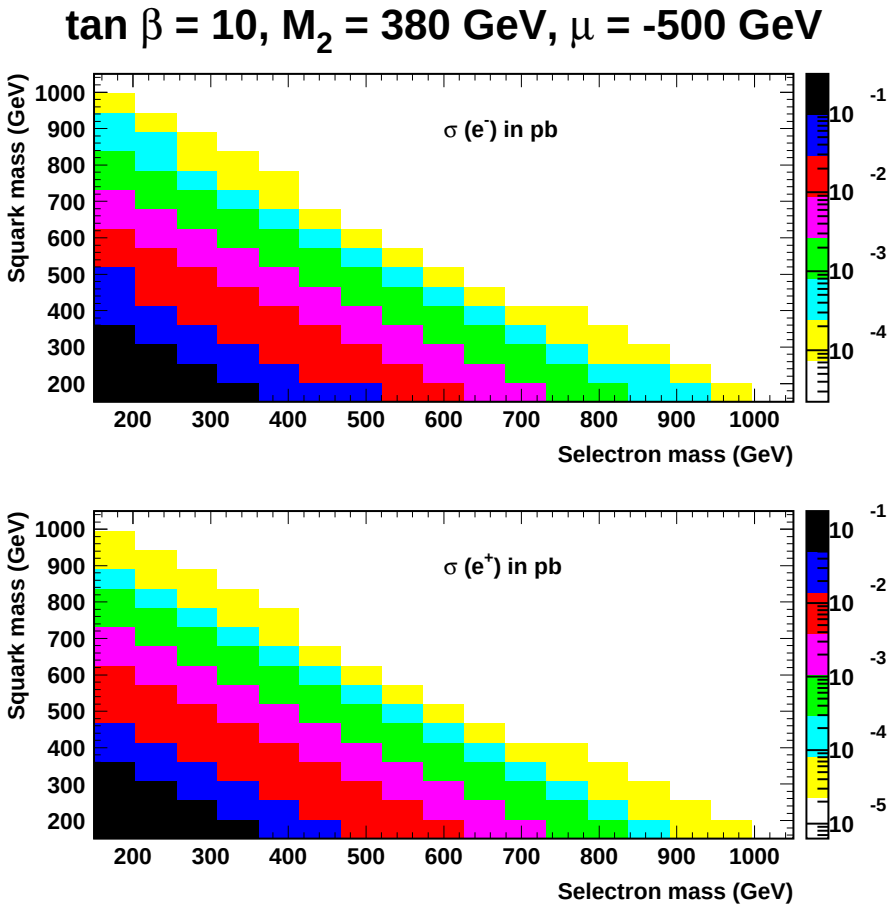

Figure 6: Production cross section (right, in pb) of a selectron-squark pair at the LHeC, for example values of MSSM parameters. It is assumed that $\tilde{u}_L$, $\tilde{u}_R$, $\tilde{d}_L$ and $\tilde{d}_R$ are degenerate, as are $\tilde{e}_R$ and $\tilde{e}_L$.

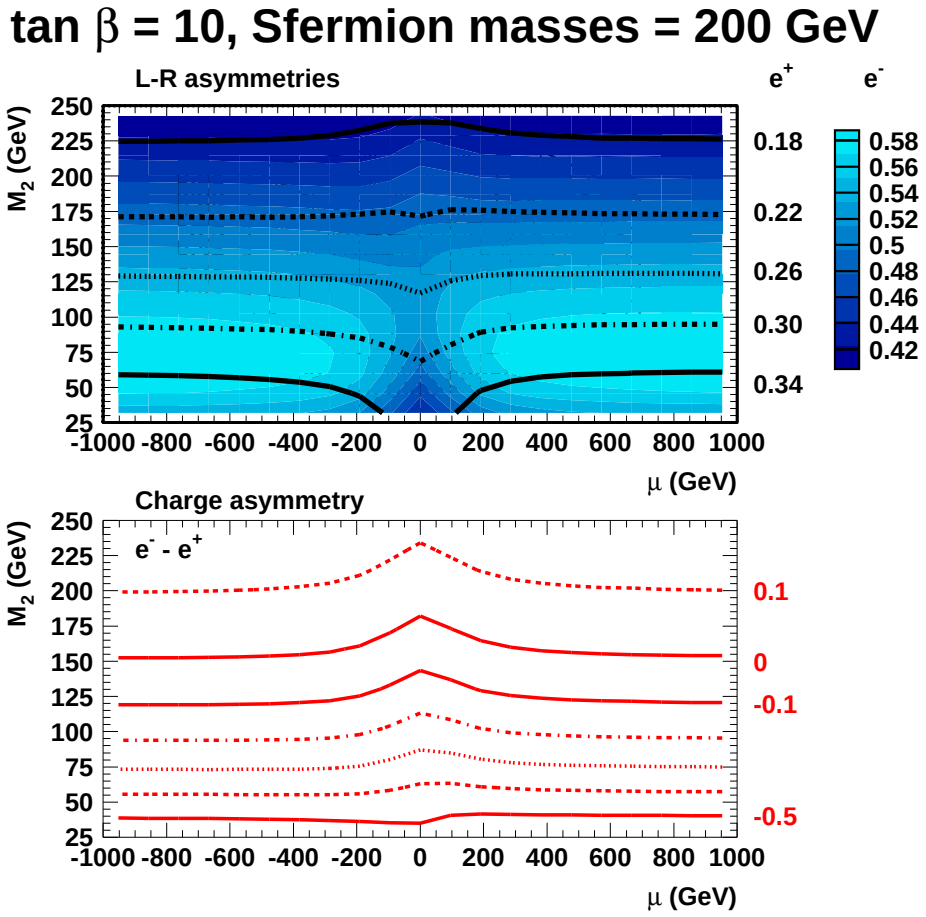

Figure 7: Polarisation (top) and charge (bottom) asymmetries of the $\tilde{e}\tilde{q}$ production cross section at LHeC in the $M_2 - \mu$ plane in the MSSM. Light sfermion masses are assumed. The numerical values on the right of the plots correspond to the asymmetry values of the contours.

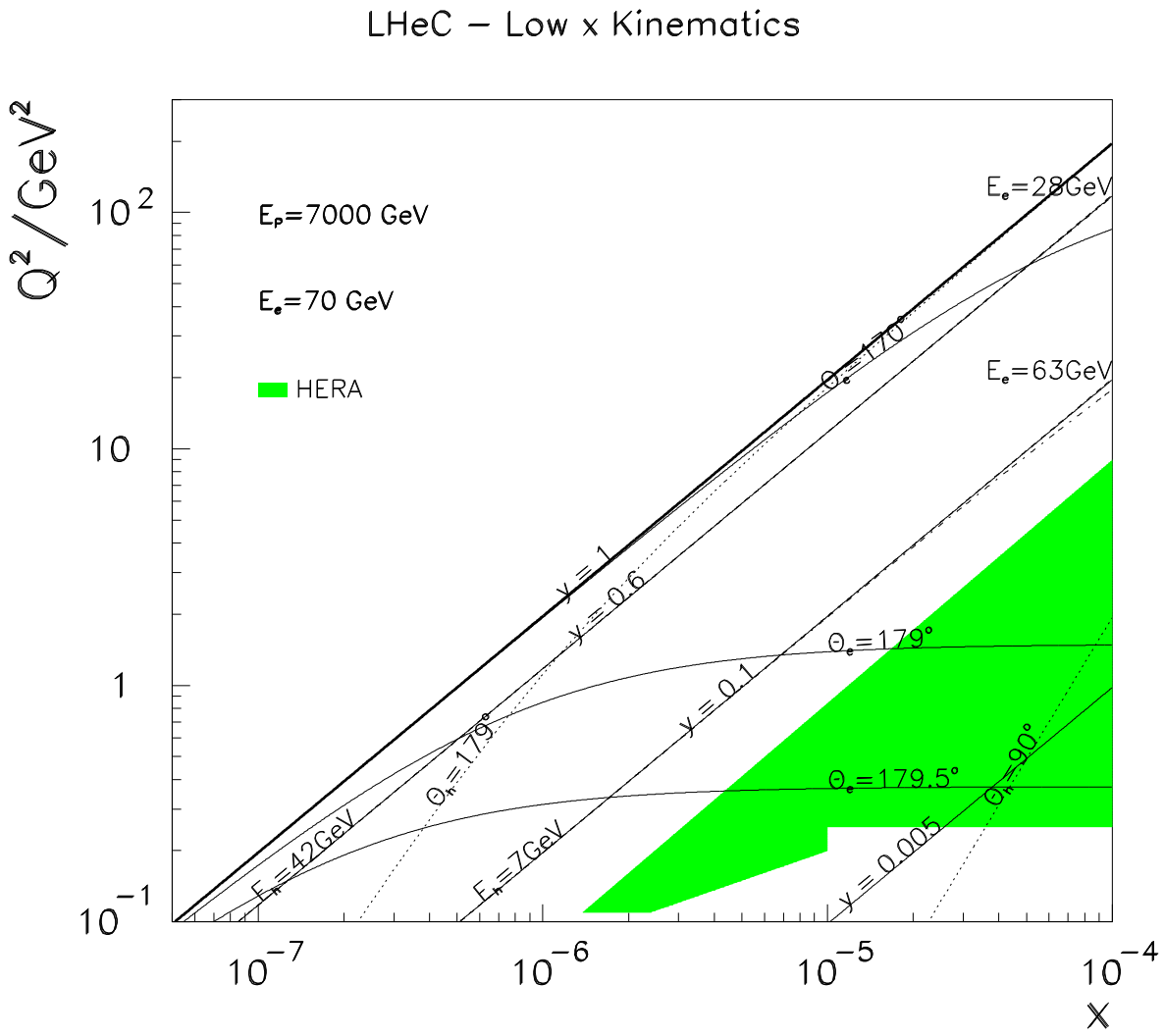

Figure 8: Kinematics of ep scattering at the LHeC at low x. Access to the Q^2 region down to $1\,\mathrm{GeV}^2$ requires a dedicated interaction region with acceptances extended to about 179°, with respect to the proton beam direction, i.e. an extended "backward detector". The shaded area illustrates the region of kinematic coverage in NC scattering at HERA, which below $x \sim 10^{-4}$ has been reached with special techniques, a detector attached to the beam pipe backwards from the main apparatus and also by shifting the interaction vertex into the proton beam direction.

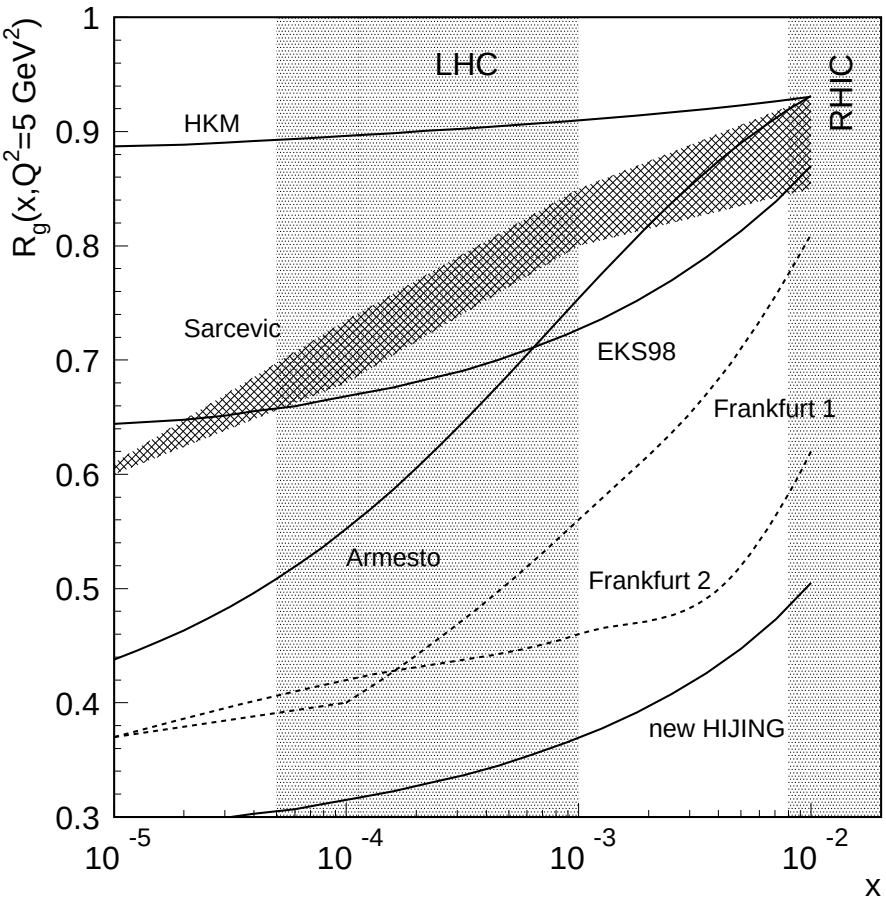

Figure 9: Ratios of gluon distribution functions in lead (Pb) relative to the gluon distribution in the proton using different models, at $Q^2 = 5\,\mathrm{GeV}^2$.

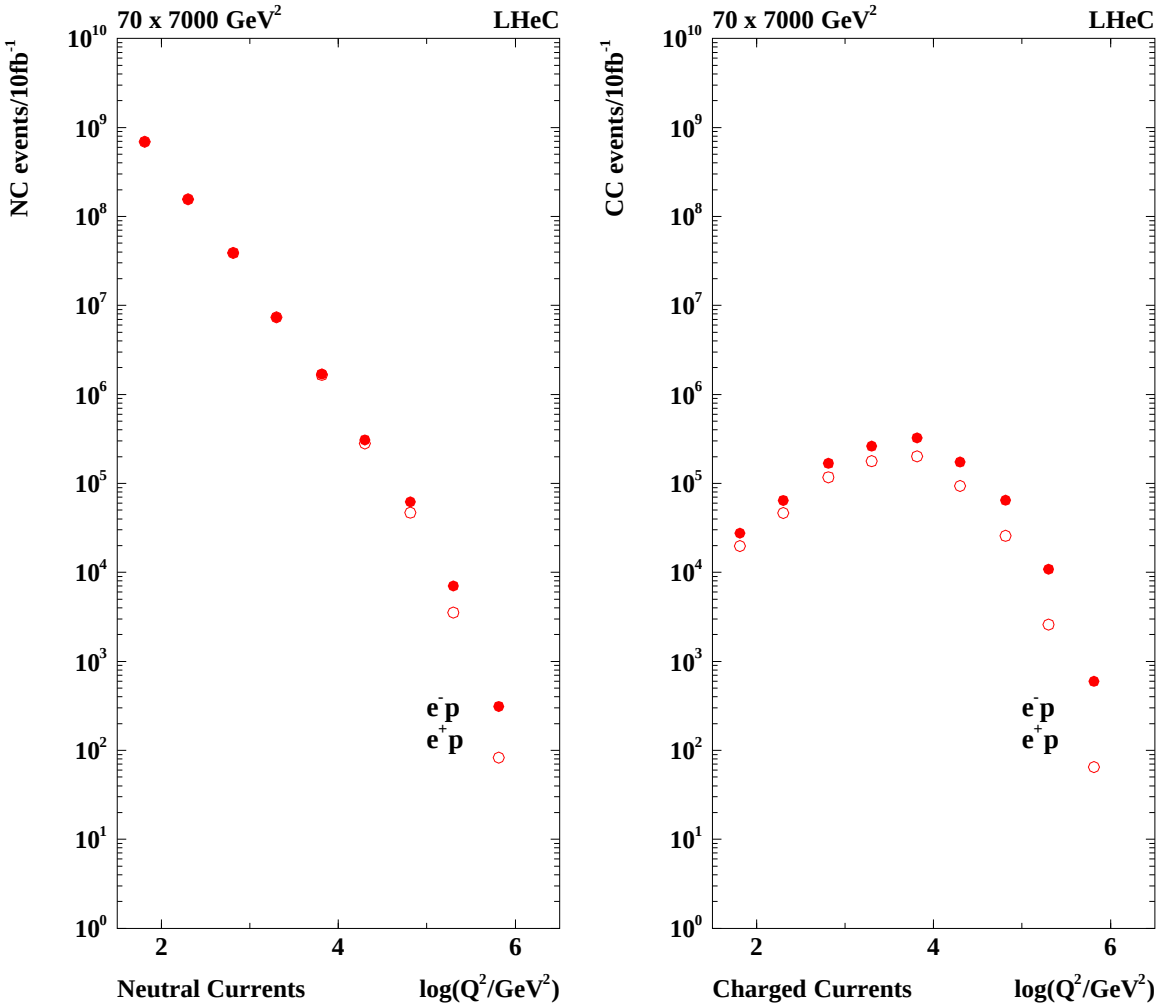

Figure 10: Event rates per 10fb^{-1} in neutral (left) and charged (right) current $e^{\pm}p$ scattering at the LHeC. At design luminosity such rates may be accumulated within one year of operating the LHeC.

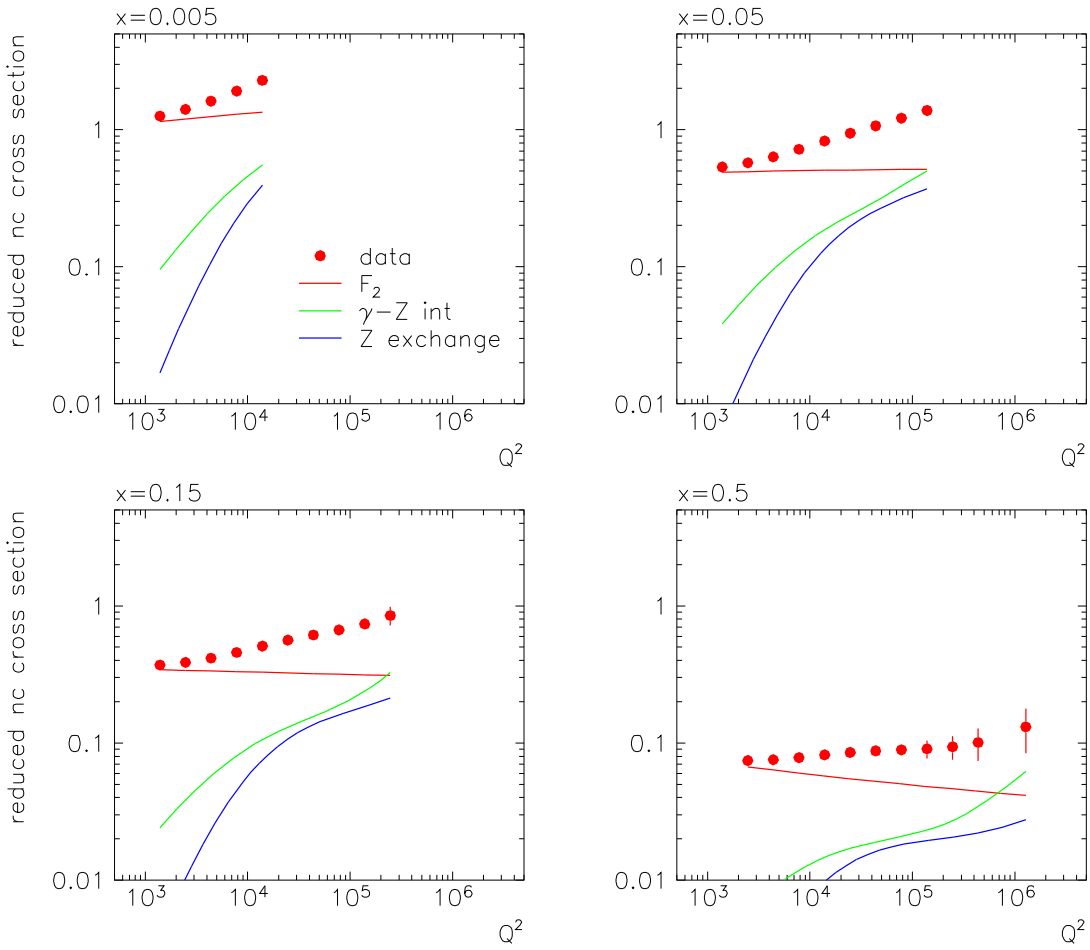

Figure 11: Simulation of a measurement of the neutral current ep scattering cross section for an integrated luminosity of $200\,\mathrm{pb}^{-1}$. Plotted is the reduced NC cross section, $d\sigma/dxdQ^2 \cdot Q^4 x/2\pi\alpha^2 Y_+$, which in the one-photon exchange approximation is equal to F_2, where $Y_+ = 1+(1-y)^2$. With rising Q^2 the effects due to the exchange of weak bosons become sizeable such that, for example, the generalised structure function F_2 is not decreasing at large x anymore, as would be the case for pure photon exchange, solid (red) line. The luminosity used here is only $200\,\mathrm{pb}^{-1}$. Accurate measurements at the LHeC in the rapidity plateau region $x \simeq 0.005$ can thus be done using data of a very short running period, less than 2 weeks at design luminosity.

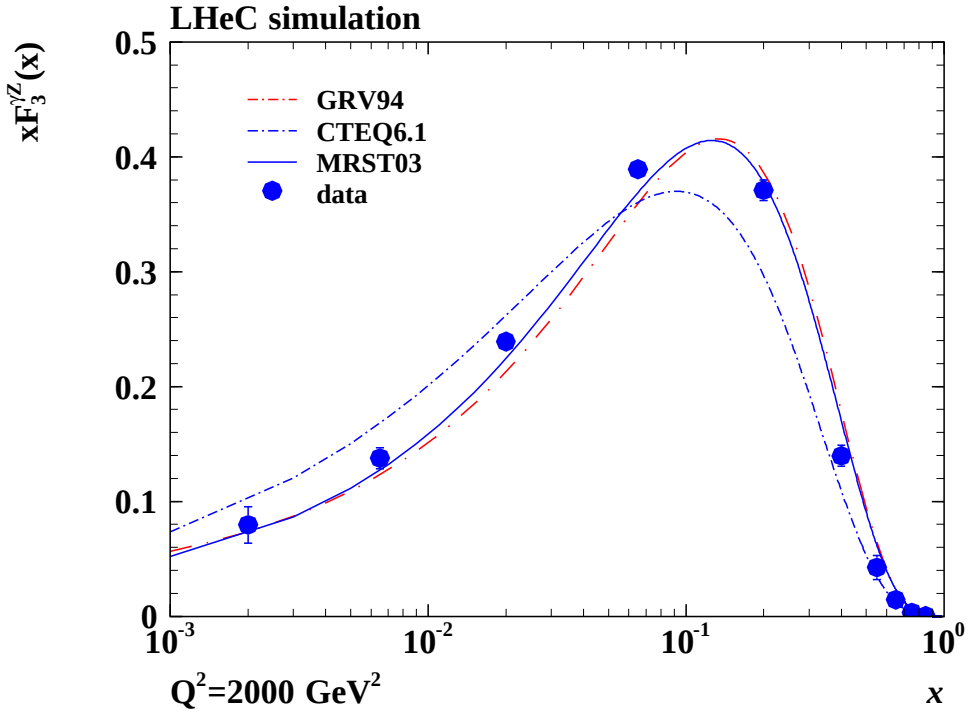

Figure 12: Simulation of a measurement of the neutral current interference structure function $xG_3 = xF_3^{\gamma Z}$ from an $e^{\pm}p$ NC charge asymmetry measurement assuming a luminosity of $10\,\mathrm{fb}^{-1}$ per beam setting. This function is defined as [38] $xG_3 \simeq 2x[a_u e_u(U - \overline{U}) + a_d e_d(D - \overline{D})]$. For the first time one thus has direct access to the antiquark-sea (a?)symmetry at low x in the deep inelastic region. In the QPM it is usually assumed that antiquarks and sea quarks are equal to each other, e.g. $\overline{u} = u_s$ and $s = \overline{s}$. This assumption is common to all pdf parameterisations used here, which therefore tend to zero at low x. Recent analyses of the NuTeV anomaly, however, suggest a possible difference between strange and anti-strange quark distributions [39]. Symmetry implies that $xG_3 = (2u_v + d_v)/3$, which is expected to drop to zero at low x and to be roughly independent of Q^2. The data points are thus projected to an average Q^2 to display the accuracy of the measurement. From the very high Q^2 region one is able to derive a measurement over 3 orders of magnitude in x. Note that this function at HERA can only be measured down to $x \simeq 0.02$ and with much less accuracy since the Q^2 values involved are smaller, i.e. electroweak effects weaker, and the luminosity is inferior to what is projected for the LHeC.

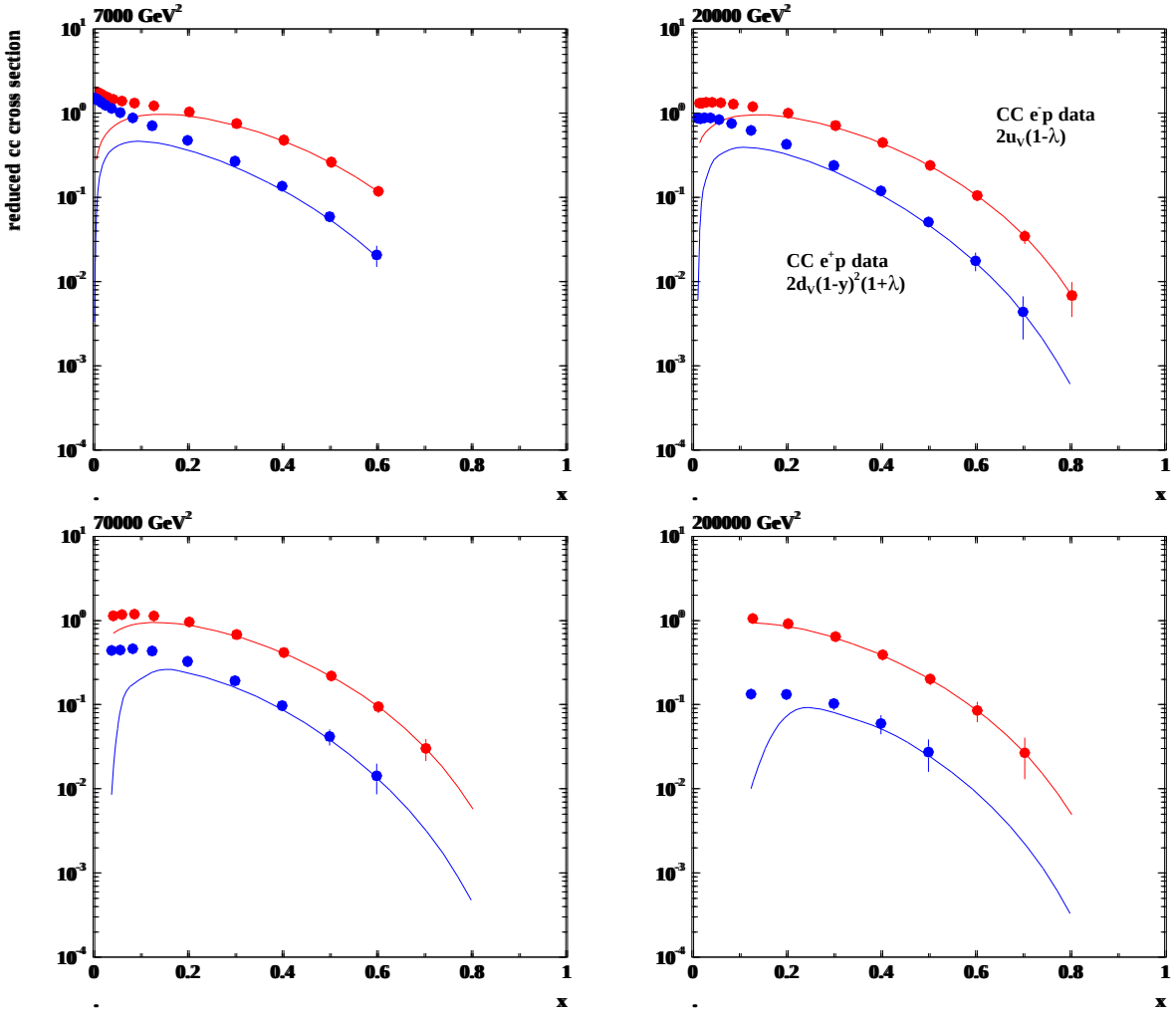

Figure 13: Reduced charged current cross sections with statistical uncertainties corresponding to $1\,\mathrm{fb}^{-1}$ in electron (top data points, red) and positron (lower data points, blue) proton scattering at the LHeC, simulated for the low x detector configuration. The curves are determined by the valence quark distributions, u_v for e^-p and d_v for e^+p using a GRV parameterisation. In the simulation the lepton polarisation λ is taken to be zero. The valence quark approximation of the reduced cross section is seen to hold already at $x \simeq 0.2$ and a rather accurate determination of the u/d ratio up to large x appears to be feasible at very high Q^2.

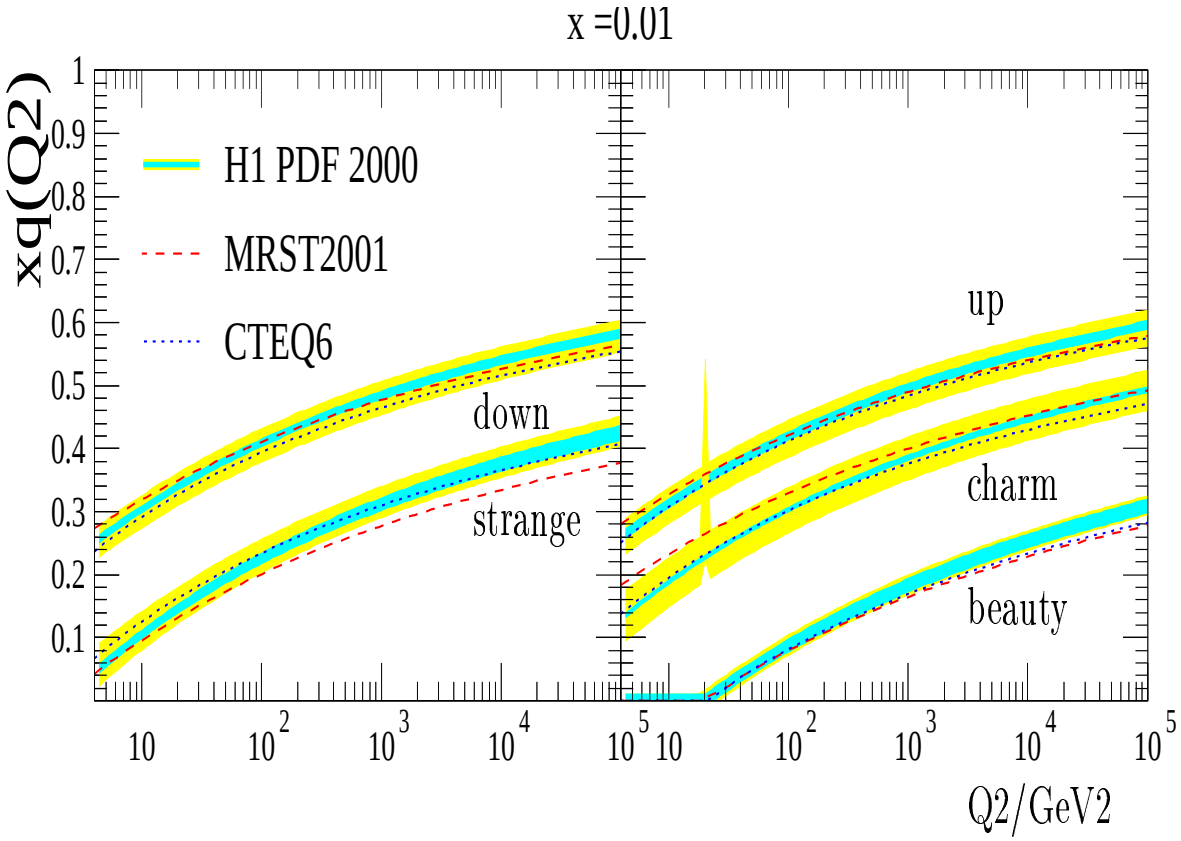

Figure 14: The Q^2 evolution of the sea quark distributions, for x within the rapidity plateau at the LHC, as predicted by NLO DGLAP pdf analyses of H1, MRST and CTEQ. At $x = 0.01$, the LHeC will cover a Q^2 range up to $10^4\,\mathrm{GeV}^2$, in which the heavy quarks distributions are becoming similarly large as the light quarks. The complete determination to high accuracy of the parton distributions is essential for searches for new physics at the LHC and also for measuring its "partonic" luminosity from the W, Z boson production rates.

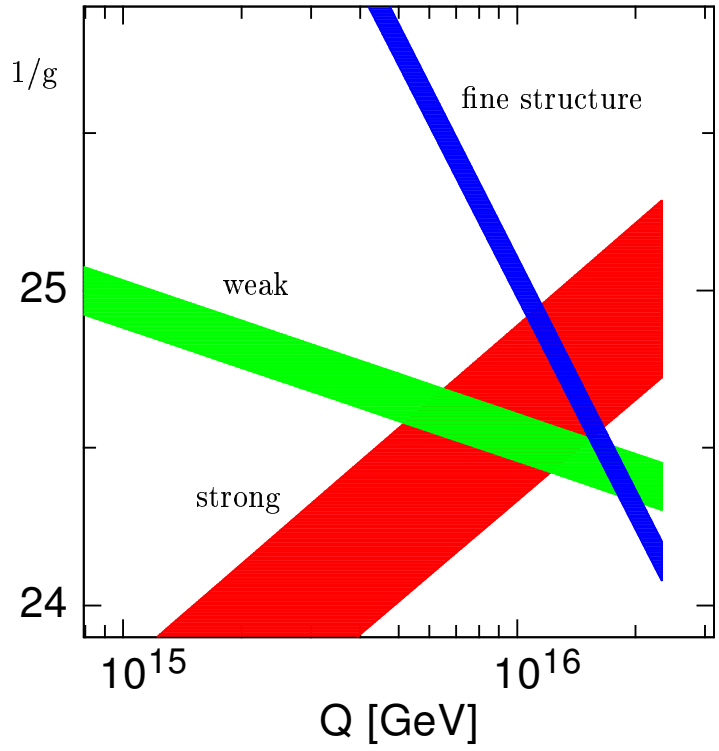

Figure 15: Two-loop extrapolation of the inverse coupling constants of $U(1)$, $SU(2)$ and $SU(3)$ to the unification point, defined as $1/g_1 = 1/g_2$, in the MSSM model using the $\overline{DR}$ scheme. The uncertainty is dominated by the rather moderate knowledge of the strong coupling constant. Improvements on the measurement of α_s are expected also from the Giga Z mode at the ILC [46].

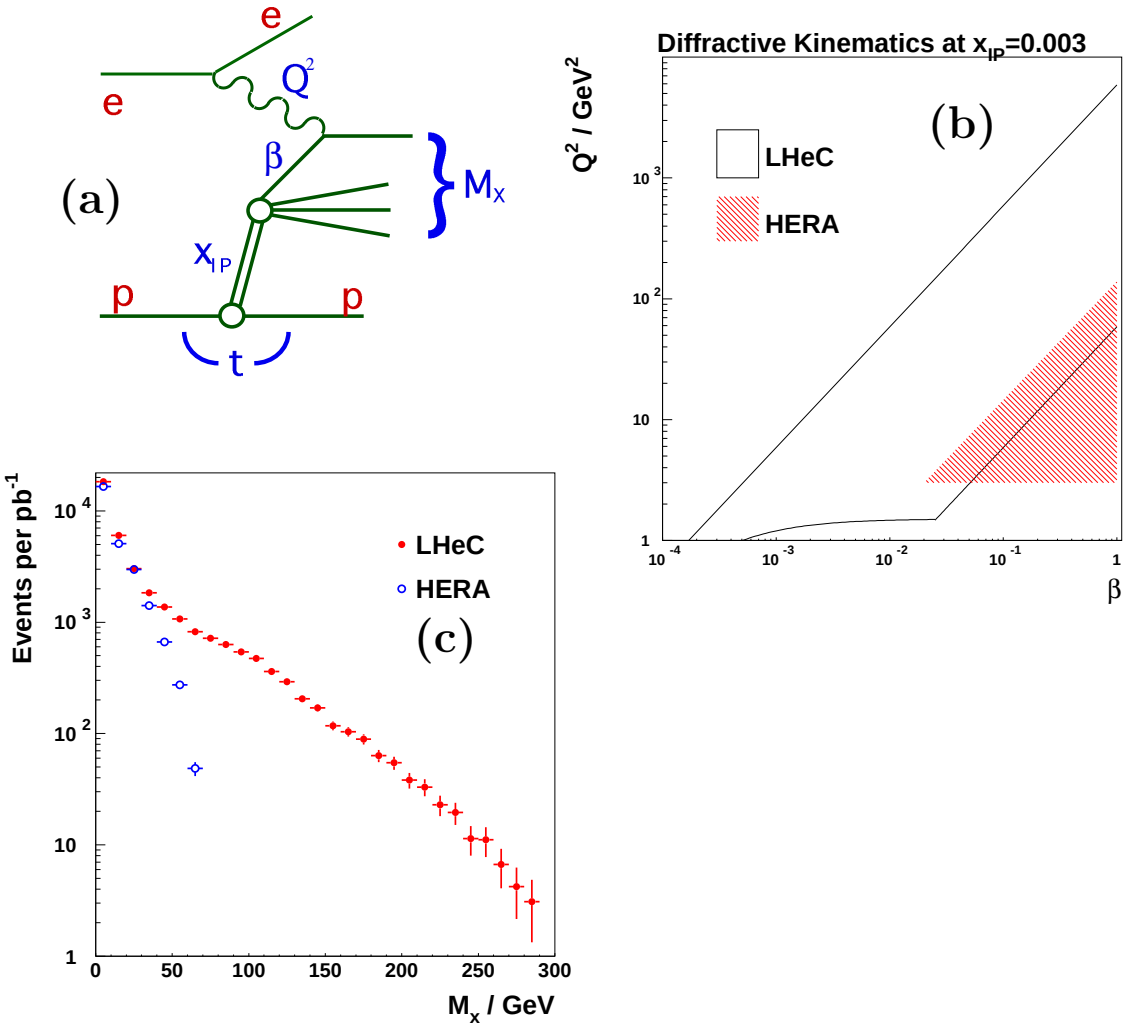

Figure 16: (a) Feynman diagram for diffractive DIS, indicating the kinematic variables used in the text. (b) Comparison of the kinematic region in β and Q^2 accessible at HERA and LHeC for an example $x_{I\!P} = 0.003$. The LHeC region corresponds to $0.01 < y < 1$ and $\theta'_e < 179°$. Similar extensions are available over the full range of $x_{I\!P} < 0.05$ which is relevant to diffraction. (c) Monte Carlo simulation, comparing the diffractive mass distributions at HERA and the LHeC available for studies of the hadronic final state with the selection $Q^2 \geq 3$ GeV^2, $0.1 < y < 0.9$ and $x_{I\!P} < 0.05$.

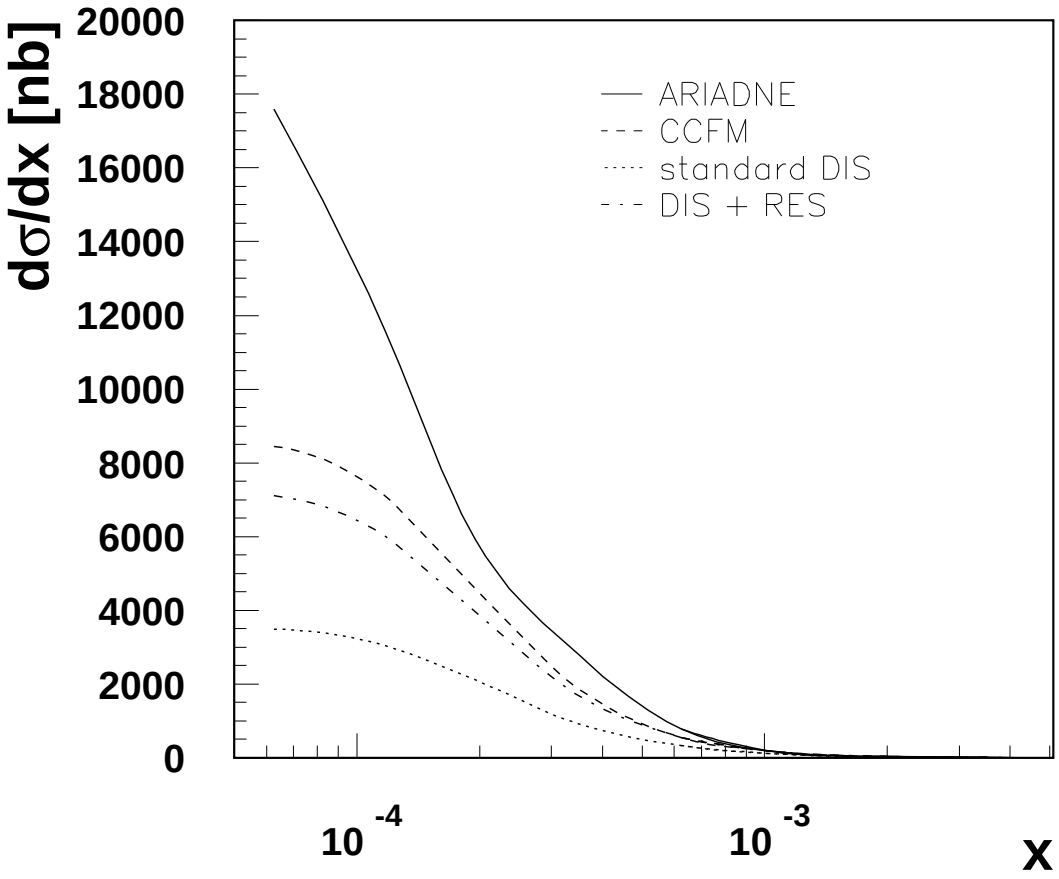

Figure 17: Forward jet cross section as a function of x in different models for the pattern of parton radiation, for $0.5 < p_T^2/Q^2 < 2$ and minimum polar jet angle of 1° as is envisaged for the low x IR. The measurements at HERA are limited to $x \geq 2 \cdot 10^{-3}$, a range, in which the resolved photon effects may still mimic non k_t ordered parton emission. The predictions of ARIADNE and the CCFM equation become largely different only at x, i.e. below the kinematic range accessed by HERA, see [9].

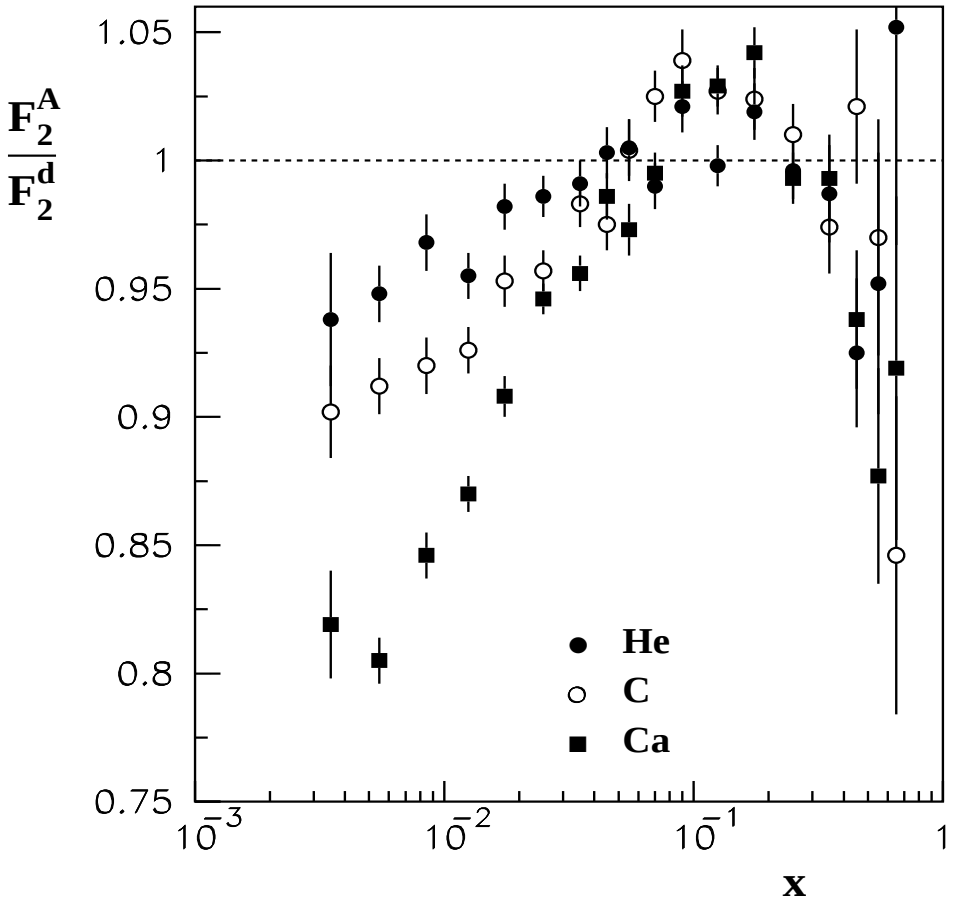

Figure 18: Ratio of F_2 structure functions in nuclei to deuteron as measured in fixed target muon scattering by the NMC Collaboration. At the LHeC this measurement can be extended down to nearly $x = 10^{-6}$ in the deep inelastic region. Note that the Q^2 values at the smallest $x \simeq 3 \cdot 10^{-3}$ in this plot are below $1\,\mathrm{GeV}^2$ for the NMC but reach a few $1000\,\mathrm{GeV}^2$ at the LHeC.

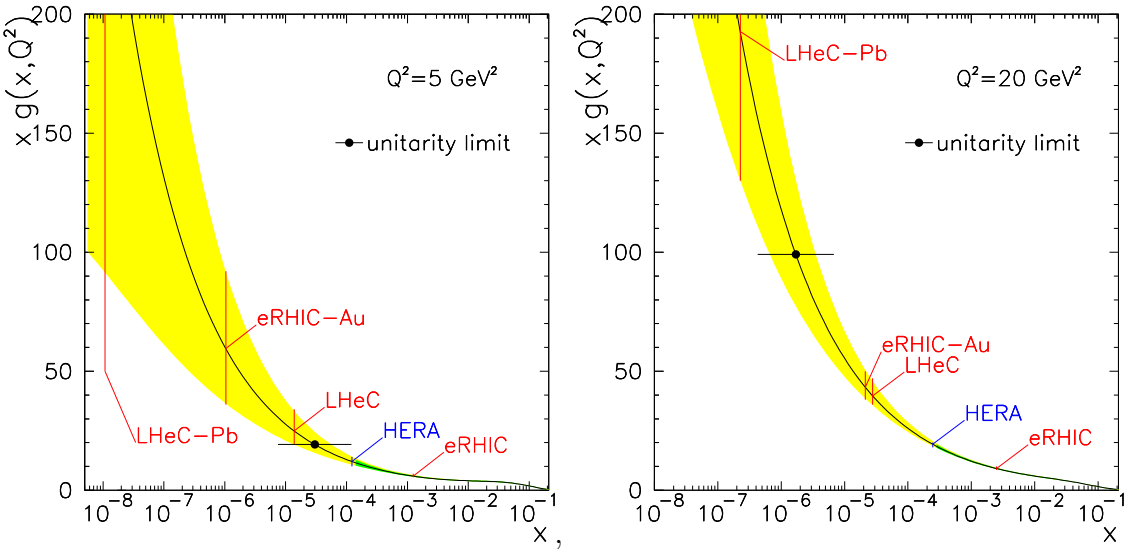

Figure 19: The gluon distribution as determined in an NLO DGLAP QCD analysis of H1 data extrapolated from the accessed region above 10^{-4} to much lower values of Bjorken x, for $Q^2 = 5\,\mathrm{GeV}^2$ (left) and $Q^2 = 20\,\mathrm{GeV}^2$ (right). The gluon distribution is expected not to rise strongly beyond the unitarity limit, which is estimated to be of the order of $Q^2/\alpha_s(Q^2)$ (solid points). The extension of the kinematic range by the LHeC leads beyond the unitarity limit at lower Q^2 in ep scattering and also for larger Q^2 in eA scattering, when the increase of the gluon density in nuclei $\propto A^{1/3}$ is taken into account, considering here ePb scattering. Due to the much higher energy, the LHeC explores a much smaller region of x than is accessible by eRHIC in eAu scattering. A clear observation of saturation in ep scattering at the LHeC will be crucial in distinguishing saturation phenomena from nuclear effects in eA and AA interactions.

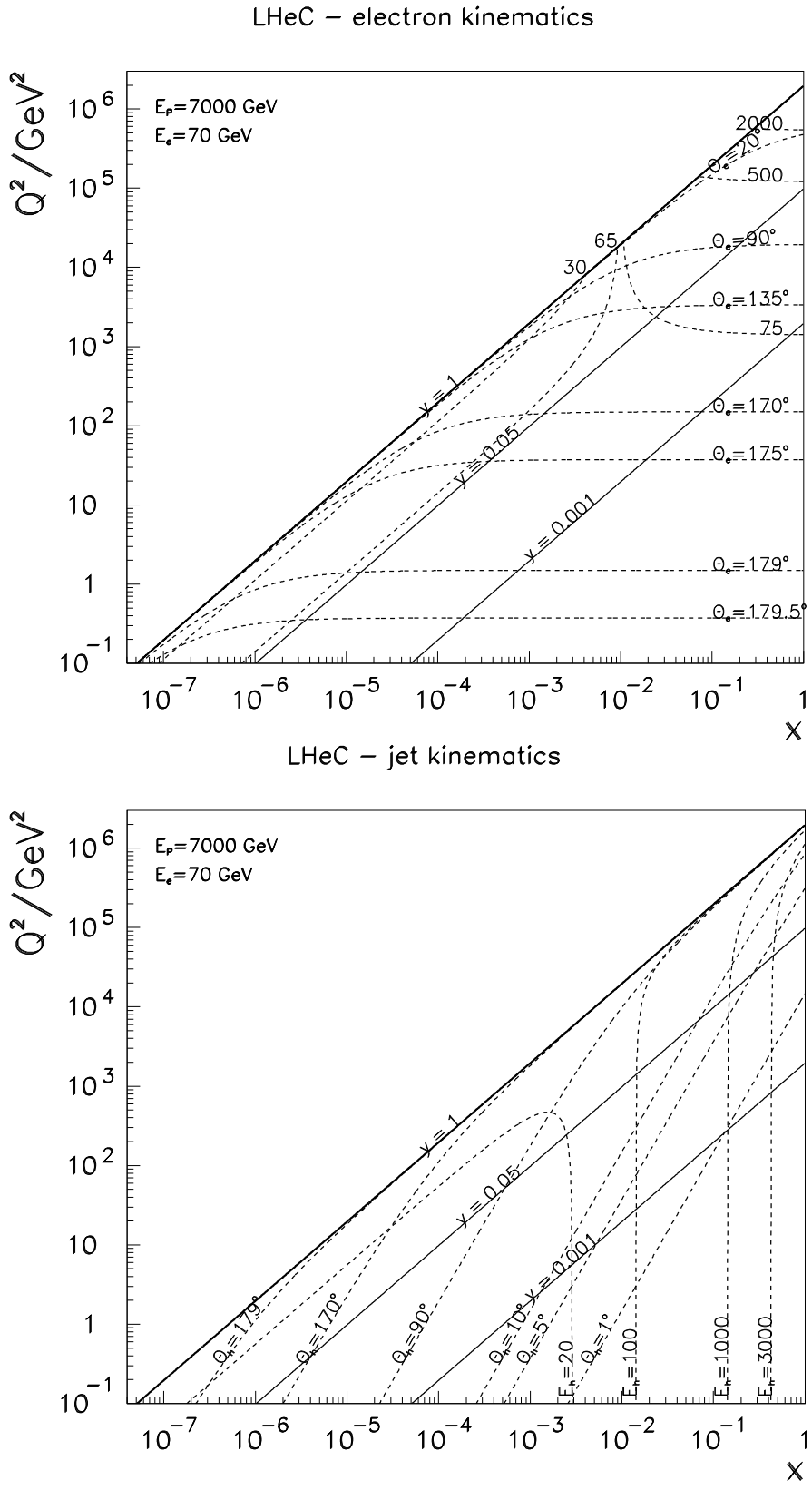

Figure 20: Kinematics of electron (top) and hadronic final state, jet (bottom) detection at the LHeC.

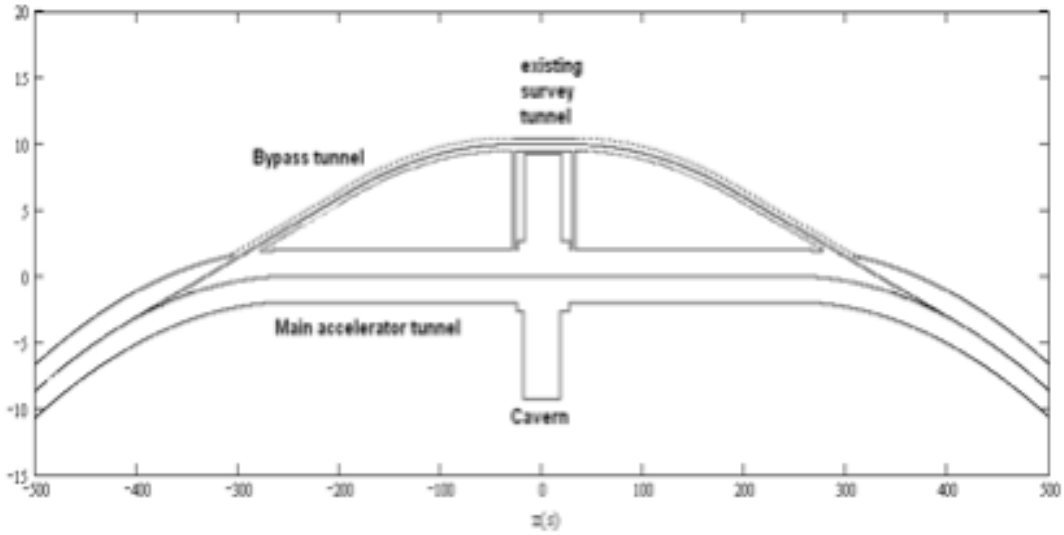

Figure 21: Top view (schematically) of straight section around IP1 (IP5) with an e-ring bypass around the experimental caverns of ATLAS and CMS, the scales are in meters.

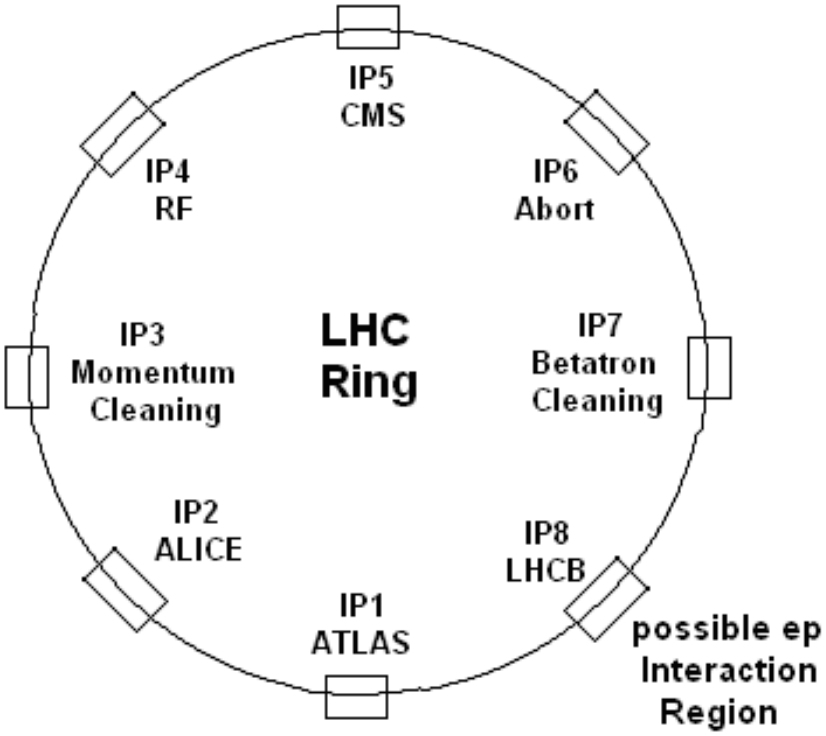

Figure 22: Possible location for the lepton-proton interaction region assuming that the B physics programme may be finished when the LHeC can be installed.

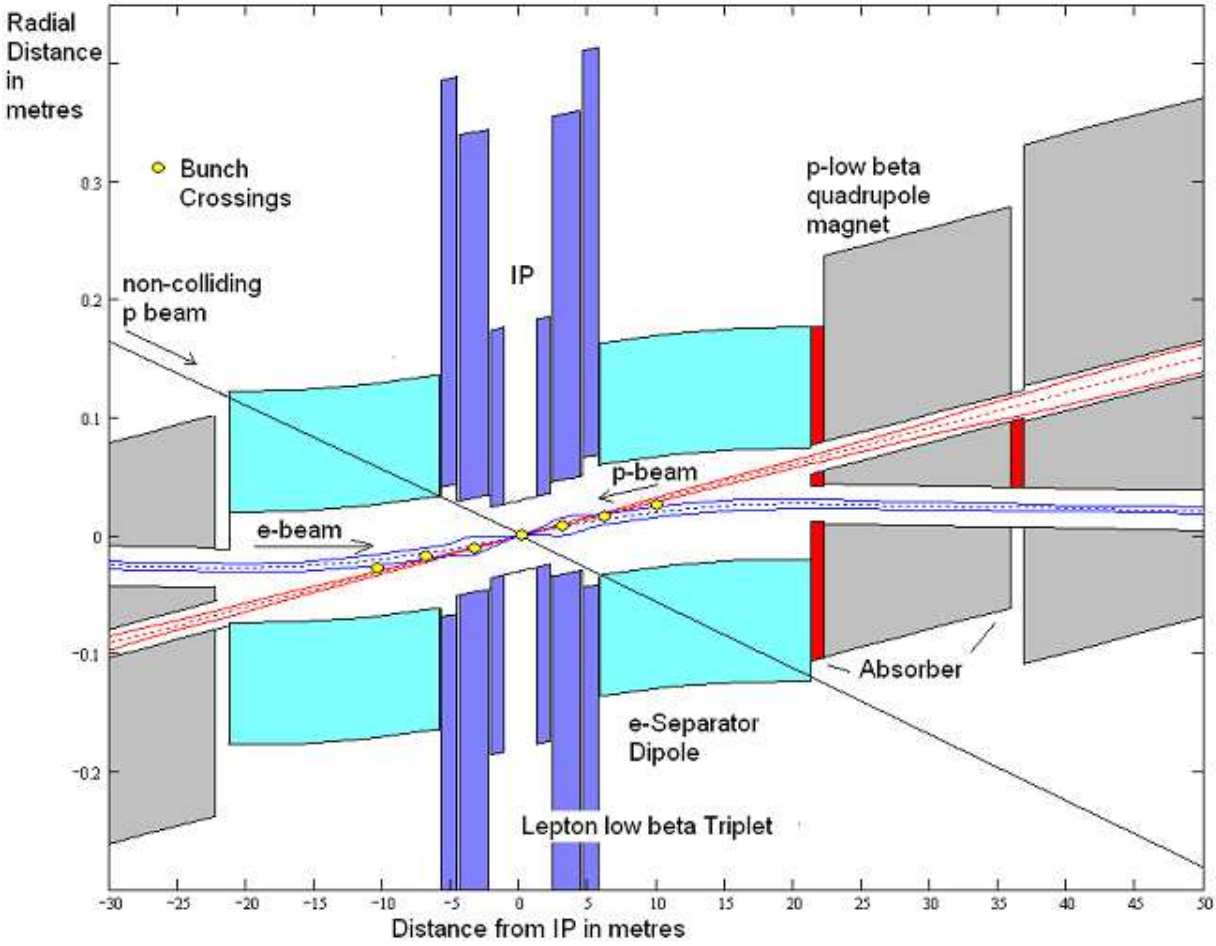

Figure 23: Top view (schematically) around the IP, the 15 σ beam envelope of the proton and the lepton beams are shown, the non-colliding proton beam envelope is not shown.

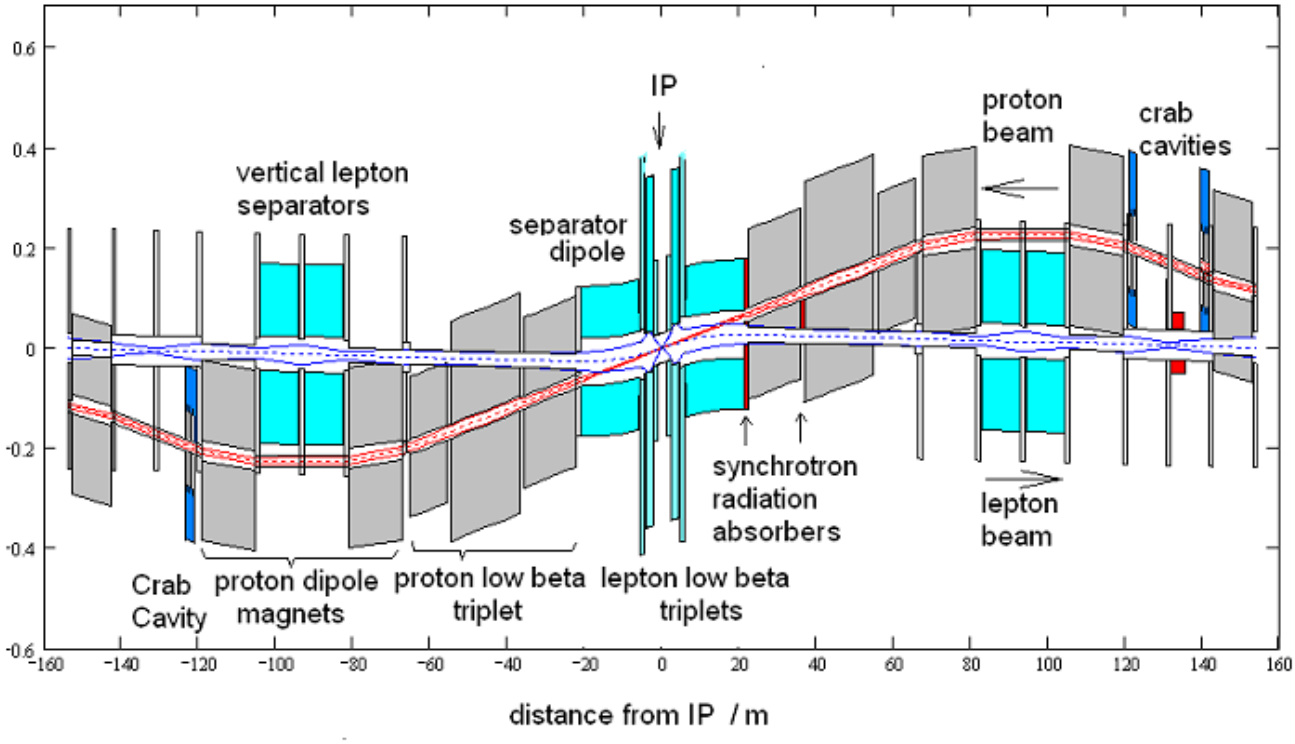

Figure 24: IR conceptional overview (top view)

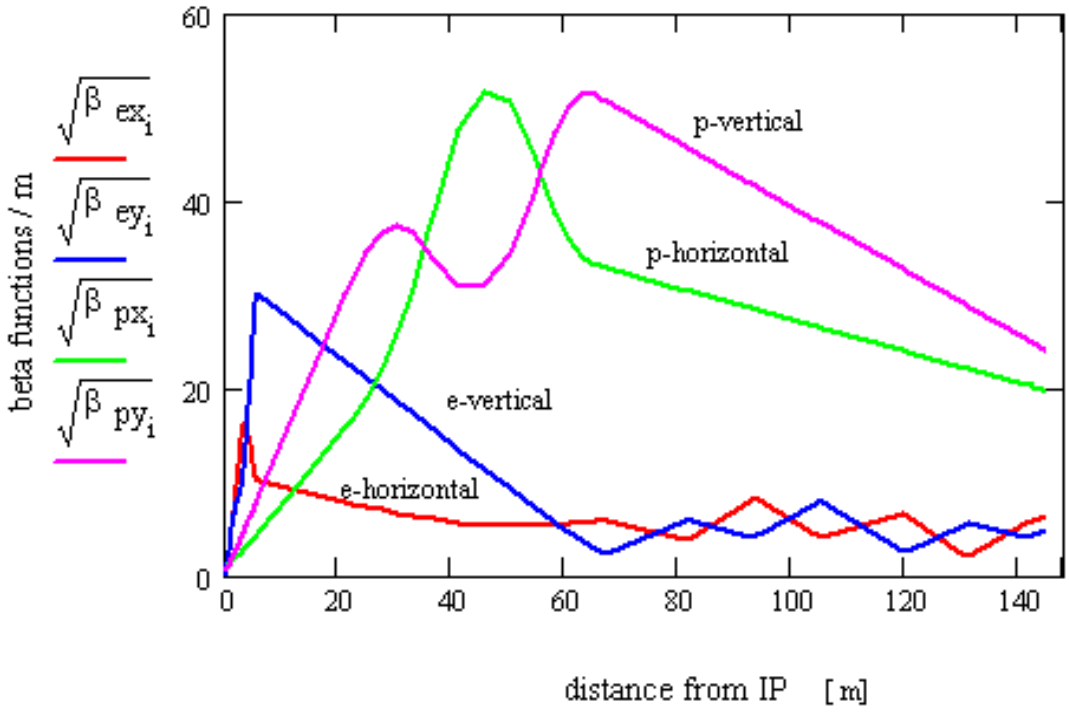

Figure 25: Lattice functions for the proton and lepton beam in the lepton-proton IR.

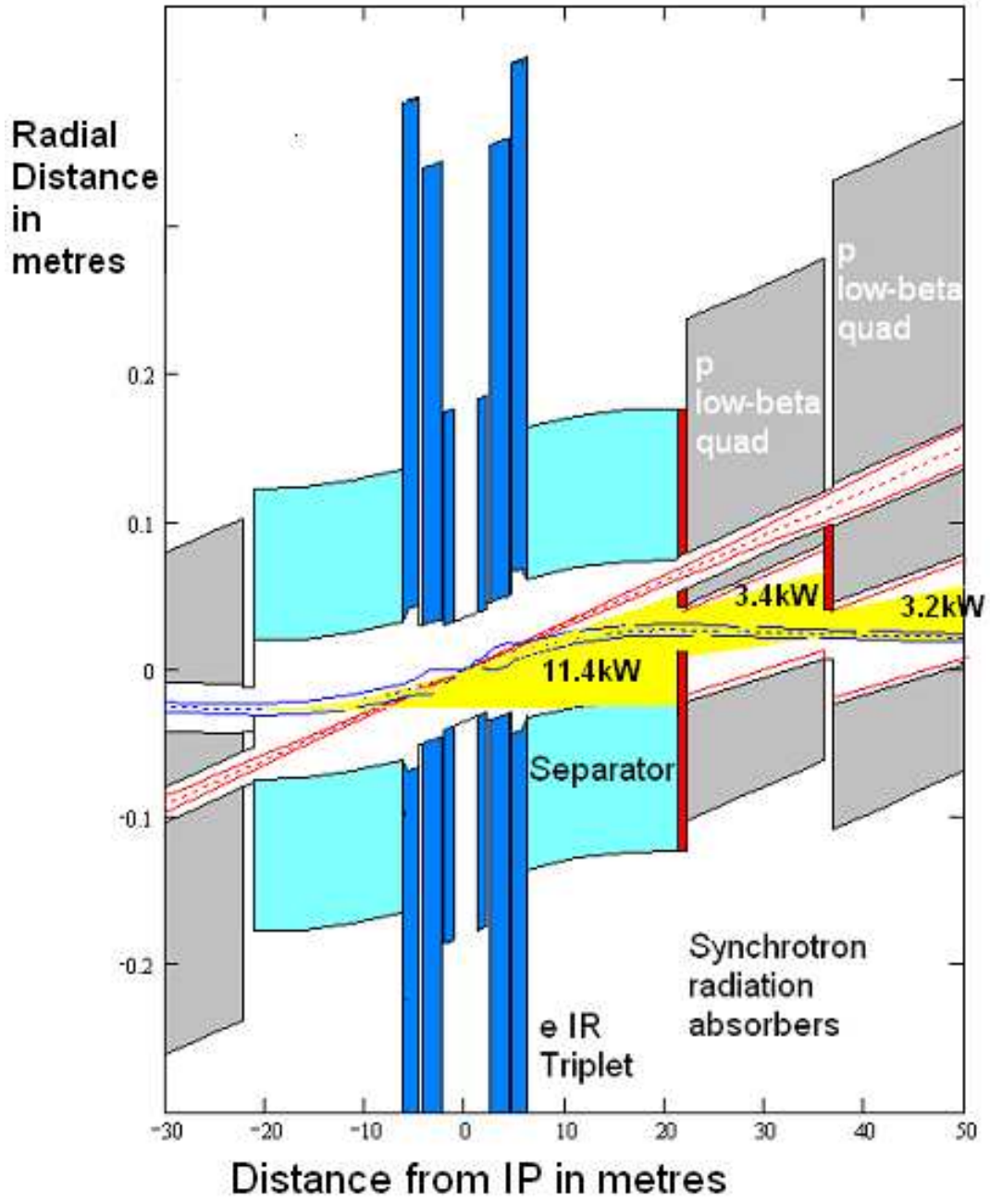

Figure 26: Deposition of Synchrotron radiation: Most of the power of 18 kW in the synchrotron radiation fan (shown in yellow) is absorbed at the collimator-absorber at 22 m from the IP (dark/red). No direct radiation is deposited inside the superconducting magnets.

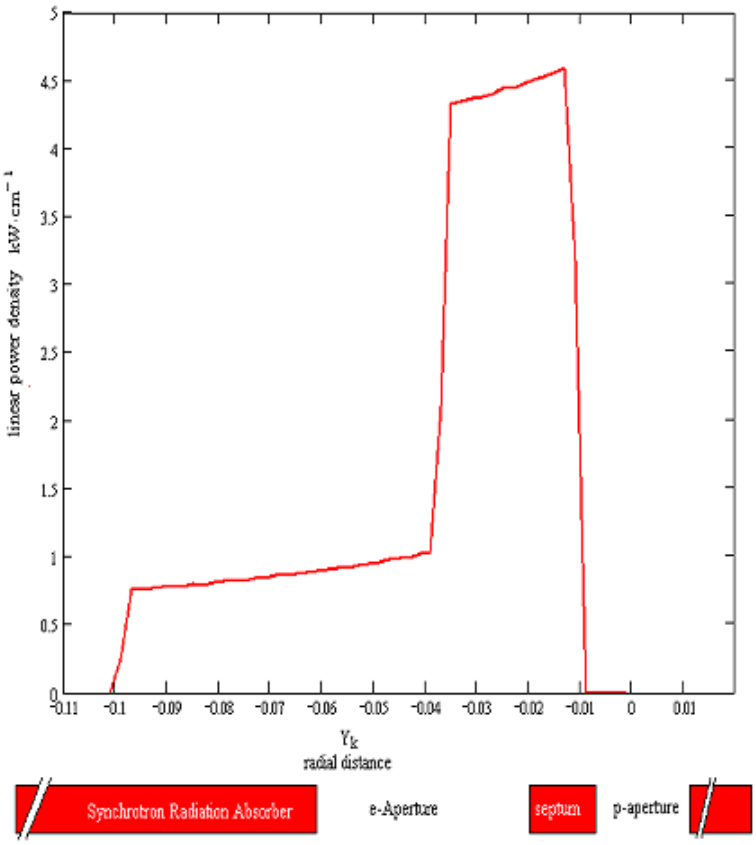

Figure 27: Linear synchrotron radiation linear power density at 21 m from the IP, at the entrance of the absorber. The red boxes below the curve indicate the position of the absorber elements.

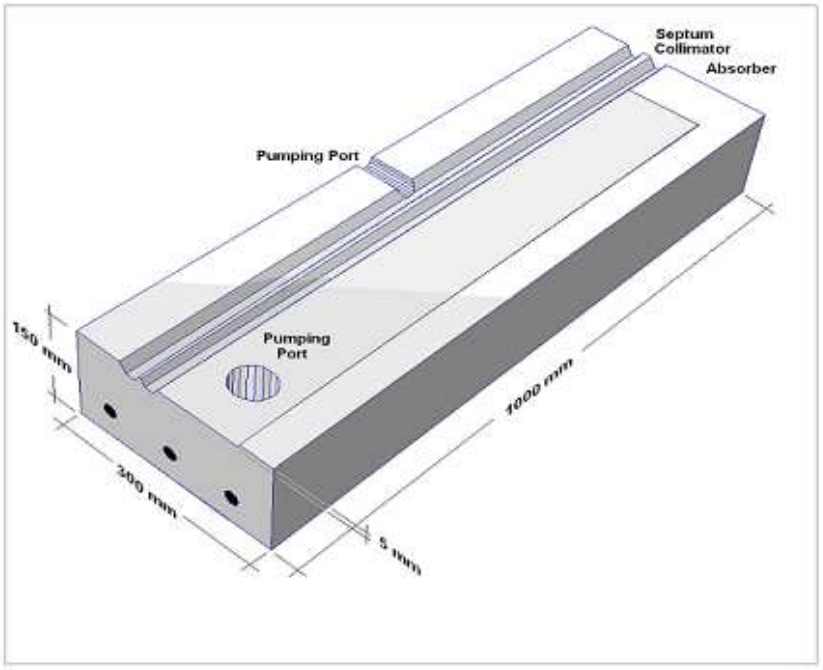

Figure 28: Sketch of the HERA-type, conical, 100 cm long, 30 cmx30 cm cross section, water-cooled synchrotron radiation absorber (cooling channels not shown) made of copper. The radiation is absorbed over a length of 400 mm and the full width of 90 mm of the absorber (shown is only the lower half of the absorber).

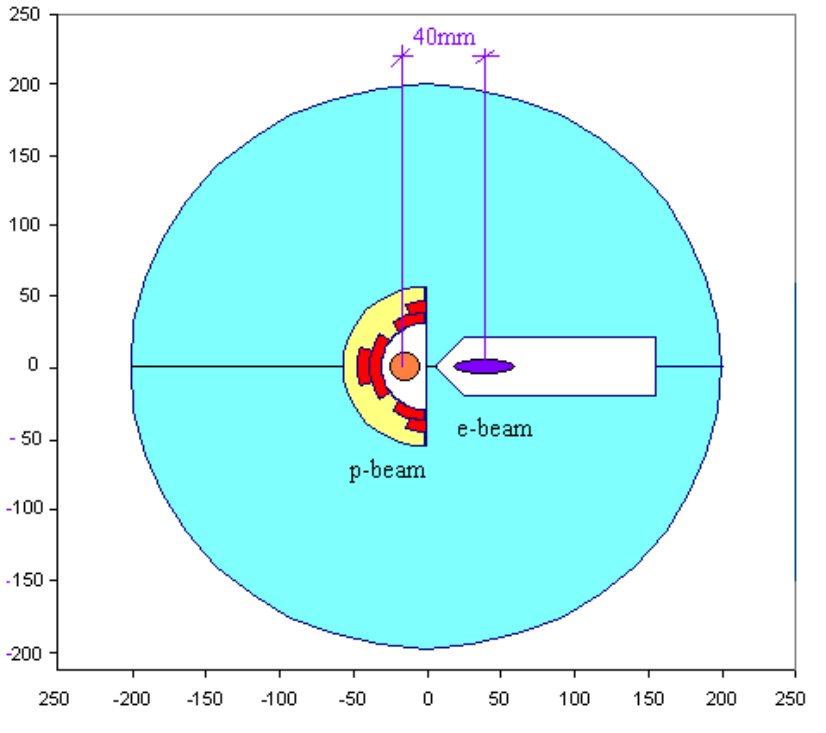

Figure 29: Sketch of the cross section of the 30 mm aperture septum quadrupole used for the vertical low beta lend of the proton beam.

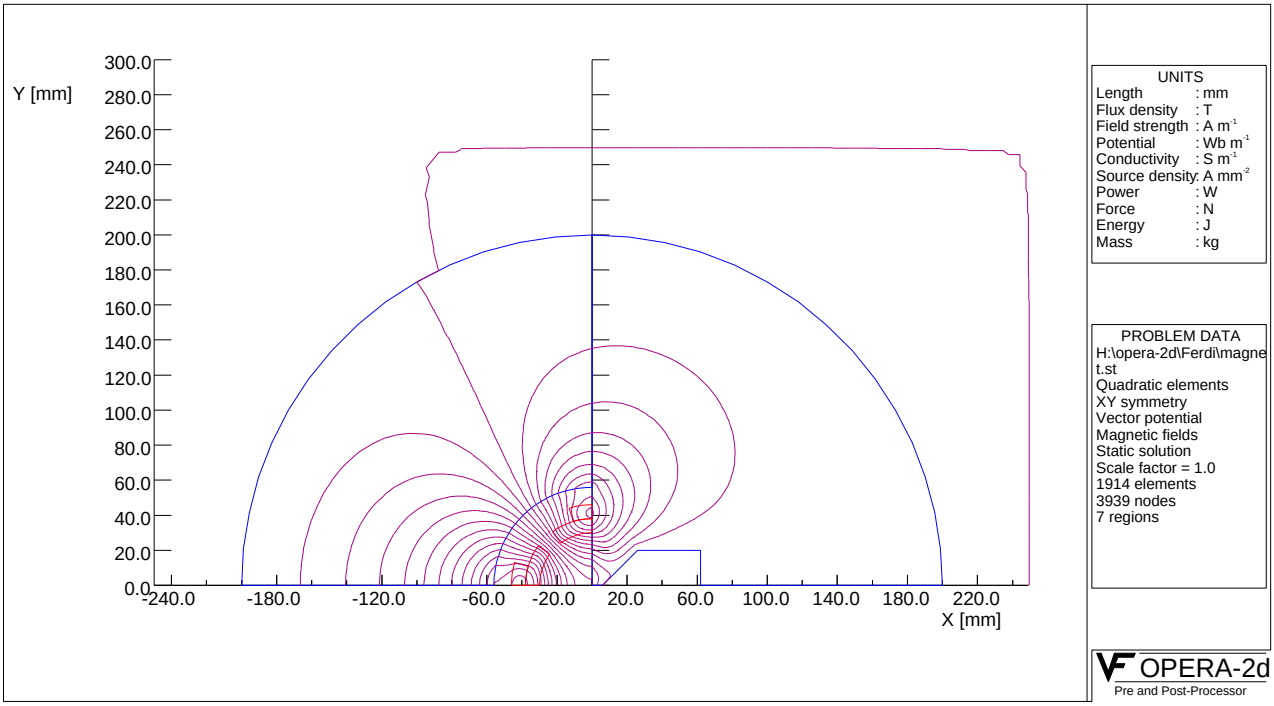

Figure 30: Field lines of the septum quadrupoles as calculated with OPERA-2D [22].

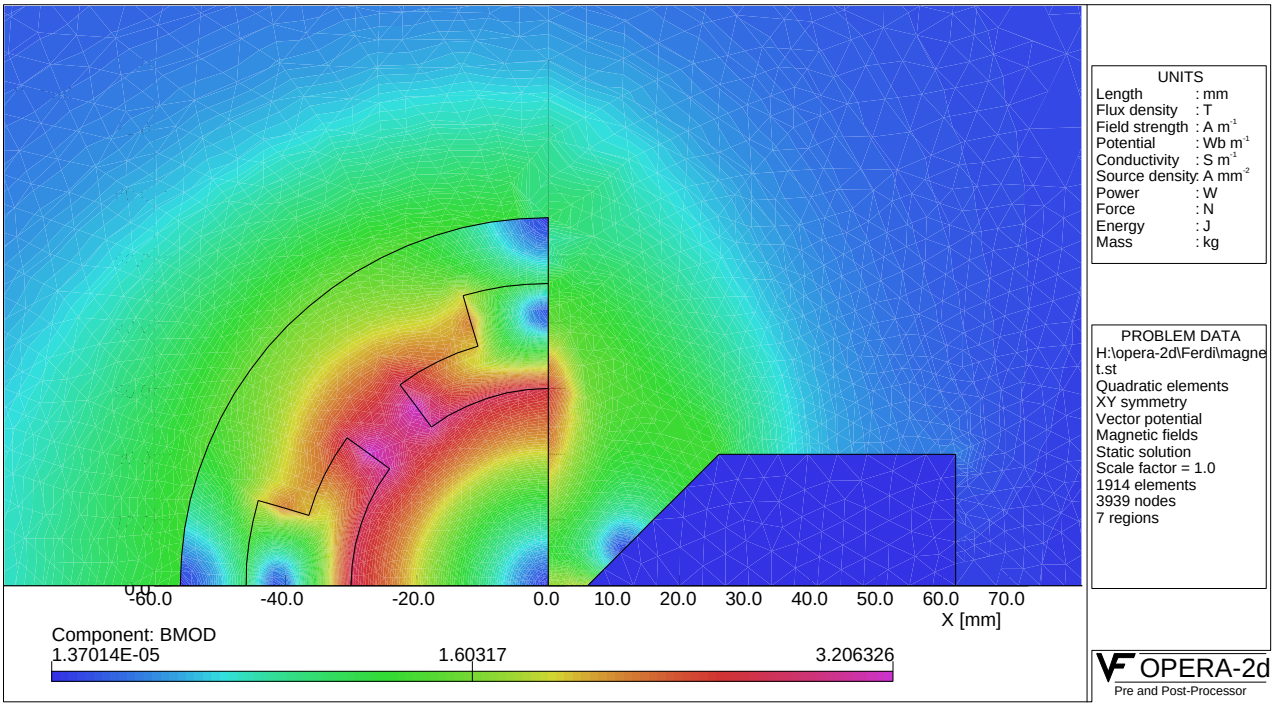

Figure 31: Field map of the septum quadrupole with OPERA-2D [15]. The magnetic induction does not exceed values of 1.6 T and the mirror plate functions well for this magnet. The magnetic field inside the septum gap is only a few gauss.